bioRxiv preprint doi: https://doi.org/10.64898/2026.04.01.715868; this version posted April 3, 2026. The copyright holder for this preprint (which was not certified by peer review) is the author/funder. All rights reserved. No reuse allowed without permission.

New three-dimensional preclinical models to understand and treat liver cancers activated for the β-catenin pathway

Short title: Tumouroids for β-catenin-activated liver cancers

Vanessa Bou Malham[1,2,3,4*], Fanny Léandre[1,2,3], Akila Hamimi[1,2,3], Isabelle Lagoutte[5], Sandrine Bouchet[1,2,3,6], Angélique Gougelet[1,2,3], Sabine Colnot[1,2,3], Christèle Desbois-Mouthon[1,2,3*]

[1] INSERM, Université Paris Cité, Sorbonne Université, Centre de Recherche des Cordeliers, F-75006 Paris, France

[2] Team « Oncogenic functions of beta-catenin signaling in the liver », Équipe labellisée par la Ligue Nationale contre le Cancer, F-75013 Paris, France

[3] AP-HP, Institut du Cancer Paris CARPEM, F-75015 Paris, France

[4] Projet de recherche Enfants, Adolescents et Cancer Ligue Contre le Cancer

[5] INSERM, CNRS, Université Paris Cité, Institut Cochin, Plateforme Imagerie du vivant, F-75014 Paris, France

[6] AP-HP, Hôpital Saint-Antoine, F-75012 Paris, France

[*] **Corresponding authors:**

christele.desbois-mouthon@inserm.fr; vanessa.bou-malham@inserm.fr

Key words: Hepatocellular carcinoma, hepatoblastoma, tumouroid, organoid, bioreactor, 3D culture

Electronic word count: 6,445

bioRxiv preprint doi: https://doi.org/10.64898/2026.04.01.715868; this version posted April 3, 2026. The copyright holder for this preprint (which was not certified by peer review) is the author/funder. All rights reserved. No reuse allowed without permission.

Number of figures and tables: 7 figures and 2 tables

Conflict of interest: none

Financial support statement: This study has been supported by grants from Institut National de la Santé et de la Recherche Médicale (INSERM), Association Française pour l'Etude du Foie (AFEF, to CDM), Institut National du Cancer (to CDM and VBM, PLBIO 24-107, and to SC and VBM, PlBio 21-268, INCa_1602), and Ligue Nationale Contre le Cancer (to SC and VBM, AAPEAC2022.LCC/VM). VBM salary is funded by Ligue Nationale Contre le Cancer (AAPEAC2022.LCC/VM, INCa_1602 PlBio21-268, and by INCa PlBio 24-107).

Authors contributions: C.D.-M. and V.B.M. conceived the study and supervised all aspects of the project. V.B.M., F.L. and A.G. performed hepatocyte isolation and cell culture experiments. V.B.M. and A.H. performed histology, immunodetection and RT-qPCR. I.L. performed liver ultrasonography. SB followed tumour progression by ultrasonography. A.G. managed $Apc^{lox/lox}$/TTR-Cre^{ERT2} mouse breeding. C.D.-M. and S.C. obtained funding supports. C.D.-M. and V.B.M. wrote the manuscript with contributions from all authors. All authors read and approved the final manuscript.

bioRxiv preprint doi: https://doi.org/10.64898/2026.04.01.715868; this version posted April 3, 2026. The copyright holder for this preprint (which was not certified by peer review) is the author/funder. All rights reserved. No reuse allowed without permission.

Abstract

Background & aims. Constitutive activation of the β-catenin pathway is a determining feature in the pathogenesis of two primary liver cancers, namely HCC and hepatoblastoma (HB). Activating alterations in *CTNNB1* gene and, to a lesser extent, inhibiting alterations in *APC* gene are observed in 30 to 40% of HCC cases and 80 to 90% of HB cases. For both tumours, therapeutic management is far from optimal. Therefore, relevant experimental models are needed to increase our knowledge and test new therapeutic approaches.

Methods. Organoids and tumouroids were established from $APC^{\Delta hep}$ and $\beta cat^{\Delta ex3}$ mouse models, which are clinically relevant models for β-catenin-activated HCC and mesenchymal HB. We developed a new methodological approach based on a dynamic suspension culture in a rotating bioreactor. Morphological and molecular characteristics and sensitivity to WNTinib, a treatment already successfully tested on human HCC and HB tumouroids, were evaluated by histology, immunohistochemistry, immunofluorescence, and RT-qPCR.

Results. This easy-to-implement methodology allows for the rapid generation of a large number of organoids and tumouroids that are uniform in size and show no signs of cell death in their core. The robustness of the methodology is illustrated by the maintenance of the histological architecture, cell diversity and gene expression in organoids and tumouroids in comparison with the native liver tissues. In addition, the value of the HCC-derived tumouroids for evaluating cancer treatment was assessed based on their responsiveness to the β-catenin antagonist WNTinib.

Conclusions. The organoids and tumouroids that we present here are new reliable *in vitro* cancer models, recapitulating the main features of β-catenin-driven HCC and mesenchymal HB. They can be integrated into an appropriate platform for drug

bioRxiv preprint doi: https://doi.org/10.64898/2026.04.01.715868; this version posted April 3, 2026. The copyright holder for this preprint (which was not certified by peer review) is the author/funder. All rights reserved. No reuse allowed without permission.

screening and could enable the development of “à la carte” therapies that are urgently needed for these indications.

Impact and implications

This study addresses the critical need for representative *in vitro* models to investigate β-catenin-driven liver cancers. The organoids and tumouroids developed here are particularly valuable for researchers seeking robust, reproducible models that accurately reflect the cellular diversity and gene expression profiles of native liver tumours. These findings have practical applications in exploring cancer mechanisms, screening new drugs, optimizing personalized treatment strategies, and reducing reliance on animal models, which ultimately benefits patients.

Highlights

- Easy and rapid generation of mouse liver organoids and tumouroids from β-catenin activated tumours using culture in a bioreactor
- Tumouroids preserve histology, cell diversity, and gene expression of native tissue
- HCC-derived tumouroids respond to β-catenin inhibitor WNTinib
- These reliable 3D models reduce reliance on animal experiments for drug testing

bioRxiv preprint doi: https://doi.org/10.64898/2026.04.01.715868; this version posted April 3, 2026. The copyright holder for this preprint (which was not certified by peer review) is the author/funder. All rights reserved. No reuse allowed without permission.

Introduction

Oncogenic activation of β-catenin is a driving event in the development of primary liver cancers in adults and children, namely HCC and hepatoblastoma (HB), respectively. HCC is the most common primary liver tumour with > 900,000 newly diagnosed people per year in the world. Its incidence is likely to increase in the coming years, making it a major public health problem. HCC also stands at the third rank of death-related to cancer worldwide accounting for more than >830,000 deaths in 2020 (1). HB is a much rarer liver tumour but is the most frequent childhood liver cancer, developing before five years of age. HB represents 1-1.5 cases per million children and its incidence has tripled over the last 30 years (2).

In these primary liver cancers, recurrent mutations and deletions affecting *CTNNB1*, the gene encoding β-catenin, have been reported. Gain-of-function mutations in *CTNNB1* are found in 30 to 40% of HCC while gain-of-function deletions in *CTNNB1* are found in 80% of HB. Loss-of-function deletions in *APC,* a tumour-suppressor gene encoding the main negative regulator of the β-catenin pathway, have been also reported in about 3 and 10% of HCC and HB, respectively (3, 4). These alterations lead to β-catenin stabilization and accumulation in the nucleus, where it binds to the transcription factor TCF4 and regulates gene expression to promote tumour initiation and progression. β-catenin pathway-mutated HCC represents a homogenous subgroup of differentiated and low proliferating tumours whose prognosis may be better than other subtypes if diagnosed at an early stage and resected (2). Unfortunately, there is no specific treatment for advanced *CTNNB1*-mutated HCC, and it appears that oncogenic activation of β-catenin confers frequent innate resistance to the reference treatment combining immune checkpoint inhibitor plus antiangiogenic agent (5–8). The molecular and cellular basis of this resistance is still poorly

bioRxiv preprint doi: https://doi.org/10.64898/2026.04.01.715868; this version posted April 3, 2026. The copyright holder for this preprint (which was not certified by peer review) is the author/funder. All rights reserved. No reuse allowed without permission.

understood. HB demonstrates an important phenotypic diversity with three main histological subtypes presenting a spectrum of differentiation states (9) that is reflected at the transcriptomic level (2, 3, 9–13). HB is usually treated by cisplatin-based neo-adjuvant and adjuvant chemotherapy and surgical removal, leading to >80% 5-year survival (14). However, patients diagnosed with advanced unresectable tumours, chemo-resistant tumours or recurrent disease have a poorer prognosis. Chemotherapy-related toxicity is also a major concern for patients with HB (15).

For many years, our team has generated and characterized mouse models of liver carcinogenesis dependent on the β-catenin pathway. Using Cre-lox recombination and more recently CRISPR/Cas9 approaches in mice, we have demonstrated that oncogenic activation of the β-catenin pathway in hepatocytes following loss of *Apc* expression ($APC^{\Delta Hep}$ model) or stabilizing mutations in *Ctnnb1* ($\beta cat^{\Delta Ex3}$ model) is sufficient to promote cell transformation and tumour initiation (16, 17). $APC^{\Delta Hep}$ and $\beta cat^{\Delta Ex3}$ mice develop at equal risk HCC and HB-like tumours that closely recapitulate the histological and transcriptional features of human β-catenin-mutated HCC and mesenchymal HB, respectively (17). These mouse models have proven to be valuable tools for deepening our understanding of the mechanisms governing hepatocyte transformation under the control of the β-catenin pathway, as well as for testing new diagnostic and therapeutic approaches (18–20).

In recent years, three-dimensional (3D) *in vitro* culture systems have attracted considerable interest due to their potential to bridge the gap between two-dimensional (2D) culture systems and *in vivo* observations, particularly in the field of cancer (21–24). Among them, 3D tumouroids more accurately mimic the architecture and functions of the native tumour by maintaining cell-cell interaction, cell-extracellular matrix interaction, and by reproducing cellular heterogeneity and complexity of the

bioRxiv preprint doi: https://doi.org/10.64898/2026.04.01.715868; this version posted April 3, 2026. The copyright holder for this preprint (which was not certified by peer review) is the author/funder. All rights reserved. No reuse allowed without permission.

microenvironment as closely as possible. Various methods for tumouroid establishment have been developed, ranging from the simplest to the most sophisticated, such as ultra-low attachment (ULA) plate cultures, scaffold-based systems, organ-on-chips and bioreactors, each with its own advantages and limitations (25).

In this study, we sought to generate tumouroids from our clinically relevant mouse models using an original device based on dynamic suspension culture in a rotating bioreactor (ClinoStar® system, Celvivo) that favours and maintains 3D structures in a static orbit by counterbalancing gravitational forces. This technology does not require the addition of a matrix or any other type of additive that could disrupt gene expression. In addition, this culture type eliminates cell contact with plastic, minimizes shear forces due to the gentle flow of media and promotes uniform gas and nutrient exchanges. It has previously been reported that culturing the human liver cell line HepG2/C3A in the ClinoStar® produces 3D structures that are highly relevant for studying various aspects of liver pathophysiology (26–29). After optimizing the culture conditions for mouse hepatocytes activated for the β-catenin pathway, we report that this technology allows the maintenance of tumouroids derived from both HCC and HB-like mouse tumours with phenotypical and transcriptional features perfectly matching the tumours of origins. Our new 3D preclinical models show great potential for advancing both basic and translational research on β-catenin–activated liver cancers, as demonstrated by the sensitivity of HCC-derived tumouroids to WNTinib.

bioRxiv preprint doi: https://doi.org/10.64898/2026.04.01.715868; this version posted April 3, 2026. The copyright holder for this preprint (which was not certified by peer review) is the author/funder. All rights reserved. No reuse allowed without permission.

Materials and methods

Mouse models and procedures. For the generation of APC$^{\Delta hep}$ liver organoids, APC$^{lox/lox}$/*TTR-Cre^{ERT2}* mice (2-3-month-old, males) were injected intraperitoneally with 2 mg tamoxifen (MP Biomedicals) diluted in corn oil (16). High dose tamoxifen induces *Apc* deletion in around 90% of hepatocytes (**Fig.S1)**, and the subsequent activation of β-catenin-dependent pathways throughout the liver parenchyma. For the generation of APC$^{\Delta hep}$ liver tumouroids, *APC*$^{lox/lox}$ mice (2-3-month-old, males) were injected with an adenovirus encoding Cre recombinase (AdCre, 0.5 x 10^9 particles), resulting in APC loss in a fraction of hepatocytes (30-40%), subsequent β-catenin activation, and emergence of liver tumours within 4-6 months (16). For the generation of βcat$^{\Delta ex3}$ liver tumouroids, C57BL/6J mice were injected with two adeno-associated virus serotype 8 (AAV8) encoding saCas9 and sgRNA against *Ctnnb1* to promote the specific loss of *Ctnnb1* exon 3 in a subset of hepatocytes as previously reported (17). In both models, tumour development was followed by 2D-ultrasounds under anesthesia with isoflurane inhalation, as previously described (18, 19). The maximum cumulative tumour diameter permitted by the ethics committees was 12 mm and was respected. For terminal tissue and blood collection, mice were anesthetized with ketamine (80 mg/kg) and xylazine (5 mg/kg). Mice were housed on a 12/12-h light/dark cycle at 22°C-24°C with *ad libitum* access to food (Safe A03, SAFE® Complete Care Competence) and water. All animal experiments were carried out in accordance with the French government regulations and with the approval of two ethical committees (Charles Darwin, Sorbonne Université, APAFIS#16420, APAFIS#45107 and CEEA34, Université de Paris, APAFIS#14472).

bioRxiv preprint doi: https://doi.org/10.64898/2026.04.01.715868; this version posted April 3, 2026. The copyright holder for this preprint (which was not certified by peer review) is the author/funder. All rights reserved. No reuse allowed without permission.

ClinoReactor preparation. One day before their use for organoid or tumouroid culture, the humidification beads contained in the ClinoReactors (CelVivo) were hydrated with 20 ml sterile ultra-pure water (CelVivo). Then, the ClinoReactors were thoroughly washed with DPBS for 15 min before cell seeding at a rotation speed of 15 rpm as previously described (27).

Generation of hepatic organoids from APC$^{\Delta hep}$ mice. APC$^{\Delta hep}$ mouse livers were perfused with collagenase six days following tamoxifen administration, and hepatocytes and non-parenchymal cells (NPC) were isolated and counted as previously described (30). Hepatocyte viability was systematically verified by trypan blue exclusion and was greater than 90%. For 2D culture, 500,000 hepatocytes were seeded on 6-well plates coated with rat tail collagen type 1 (Gibco) in William's E medium with GlutaMAX™ (Gibco) supplemented with 10% fetal bovine serum (FBS), 100 U/mL penicillin/10 μg/mL streptomycin, 4 μg/mL insulin (Sigma-Aldrich), 0.1% bovine serum albumin (BSA) (Eurobio), 0.5 μg/mL amphotericin B (ThermoFisher Scientific), and 40 ng/mL dexamethasone (Sigma-Aldrich). Four hours later, the medium was removed and replaced with the same medium without FBS, insulin, BSA and amphotericin B. For 3D culture, hepatocytes and NPC were resuspended in William's E medium with GlutaMAX™, supplemented with 10% FBS, 50 U/mL penicillin-streptomycin, and 1% insulin-transferrin-selenium (ITS-G, ThermoFisher Scientific). For culture in 96-well ULA plates (Greiner), a mixture of 2,000 hepatocytes together with 1,000 NPC was used per well. For dynamic culture in ClinoStar®, 500,000 hepatocytes and 250,000 NPC were seeded in a ClinoReactor rotating at 45 rpm. After four days, the medium from 3D cultures was removed and replaced with the

bioRxiv preprint doi: https://doi.org/10.64898/2026.04.01.715868; this version posted April 3, 2026. The copyright holder for this preprint (which was not certified by peer review) is the author/funder. All rights reserved. No reuse allowed without permission.

same medium without FBS. The medium was then renewed every three to four days. All cultures were maintained at 37°C in a humidified atmosphere containing 5% CO_2.

Generation of hepatic tumouroids from APC$^{\Delta hep}$ and βcat$^{\Delta ex3}$ mice. The tumours were excised and immediately placed on ice in basal medium DMEM F-12 (Gibco) until processing. The tumours were then minced gently into small pieces using fine scissors, transferred to a 50-mL centrifuge tube containing 10 mL of digestion solution (0.75 mg/mL collagenase (Sigma-Aldrich) with 0.15 U dispase (STEMCELL™ technologies) in basal medium DMEM F-12) and incubated at 37°C for 20 min under gentle agitation. Three to four enzymatic digestion rounds were performed, depending on tumour size and type. After digestion, the cell mixture was filtered through a 100-µm cell strainer (Falcon) to remove aggregates and low-speed centrifuged (50 x g for 5 min at room temperature) to separate hepatocytes (pellet) from NPC (supernatant). NPC were centrifuged at 300 x g for 5 min. Hepatocytes and NPC were resuspended in 10 mL of HepatiCult™ Organoid Growth Medium (Mouse) (STEMCELL™ technologies) and seeded in a ClinoReactor. The cell suspension was cultured in the ClinoStar® at 45 rpm for up to 16 days, with the medium replaced every 3-4 days.

Organoid and tumouroid treatment with WNTinib. After 8 days of culture in the ClinoStar®, organoids and tumouroids were transferred into two ClinoReactors: one containing DMSO as a control condition and the other containing WNTinib (MedChemExpress) at 1 µM for organoids and 5 µM for tumouroids. The treatments were maintained for five days and renewed every two days.

bioRxiv preprint doi: https://doi.org/10.64898/2026.04.01.715868; this version posted April 3, 2026. The copyright holder for this preprint (which was not certified by peer review) is the author/funder. All rights reserved. No reuse allowed without permission.

Total RNA isolation, reverse-transcription and quantitative real-time PCR (RT-QPCR). Total RNA was extracted from liver tissues, organoids and tumouroids using TRIzol™ reagent (ThermoFisher Scientific) according to the manufacturer's protocol. cDNA was synthesized using Maxima reverse transcriptase (ThermoFisher Scientific). QPCR was performed with specific primers using BlasTaq™ 2X PCR master mix (abm®) or TaqMan™ gene expression assays (Applied Biosystems). The expression levels of each target gene were normalized to those of *B2m,* the most stable normalization gene under our conditions, and expressed as the relative quantity using the formula $2^{-\Delta\Delta Ct}$. For some experiments, a mixture of liver tissue cDNA served as a calibrator. PCR primer pairs and TaqMan gene expression assays are listed in **Table S1.**

Histology, immunohistochemistry (IHC) and TUNEL assay. Hematoxylin-Eosin (HE) staining, IHC and TUNEL assay were carried out on formalin-fixed paraffin-embedded liver tissue sections as previously described (19). For IHC, liver sections were deparaffinized and hydrated, and antigen retrieval was performed in citrate buffer pH 6.0 for 20 min in a water bath at 95°C. The sections were blocked with TBS with 0.1% Tween (TBST) and 5% normal goat serum (Vector Laboratories), incubated with primary antibody for 1 h at room temperature or overnight at 4°C depending on the antibody (**Table S2**), washed twice with TBST and then incubated with biotinylated secondary antibody (1:750 and 1:200 dilutions for mouse and rabbit antibodies, respectively). Immunoreactivity was detected with an avidin biotin complex–3 (VECTASTAIN® Elite ABC-HRP kit, Peroxidase, Vector Laboratories), 3,3′-diaminobenzidine system (DAB substrate kit, peroxidase (HRP) with nickel, Vector Laboratories). Nuclei were then stained with Mayer's hemalun solution, and the slides

bioRxiv preprint doi: https://doi.org/10.64898/2026.04.01.715868; this version posted April 3, 2026. The copyright holder for this preprint (which was not certified by peer review) is the author/funder. All rights reserved. No reuse allowed without permission.

were mounted after dehydration. To perform IHC on organoids and tumouroids, samples were fixed for 1 h in 10% buffered formalin (VWR) at room temperature, washed with PBS, then covered with 2% agarose in a special mould (Leica) before being embedded in paraffin. Detection of *in situ* apoptosis was performed using the terminal deoxynucleotidyl transferase dUTP nick-end labeling (TUNEL) assay, following the manufacturer's instructions (Click-iT™ TUNEL Alexa Fluor™ 647, ThermoFisher Scientific). Photographs of entire slides were captured using AxioScan Z1 scanner (Zeiss) for IHC slides, or with Eclipse E800 microscope (Nikon) and Axio Observer Z1 microscope (Zeiss) for fluorescent and TUNEL slides. The number of stained cells per field was quantified using QuPath software (31). The surface area of spheroids/tumouroids was quantified using ImageJ software.

RNA sequencing (RNA-seq) analysis. RNA-seq was performed on total RNA extracted from $APC^{\Delta hep}$ non-tumour tissues (n=5), tumours (n=5 for HCC; n=4 for HB), and tumouroids established from these tumours. Of note, two HCC (tumours 4.B and 4.G) were developed in the same mouse liver. Fastq files were then aligned using STAR algorithm (version 2.7.6a), on the Ensembl release 101 reference. Reads were then count using RSEM (v1.3.1) and the statistical analyses on the read counts were performed with R (version 3.6.3) and the DESeq2 package (DESeq2_1.26.0) to determine the proportion of differentially expressed genes between two conditions. The standard DESeq2 normalization method (DESeq2's median of ratios with the DESeq function), was used with a pre-filter of reads and genes (reads uniquely mapped on the genome, or up to 10 different loci with a count adjustment, and genes with at least 10 reads in at least 3 different samples). Following package recommendations, the Wald test was used with the contrast function and the Benjamini-Hochberg FDR control

bioRxiv preprint doi: https://doi.org/10.64898/2026.04.01.715868; this version posted April 3, 2026. The copyright holder for this preprint (which was not certified by peer review) is the author/funder. All rights reserved. No reuse allowed without permission.

procedure to identify the differentially expressed genes. R scripts and parameters are available at https://github.com/GENOM-IC-Cochin/RNA-Seq_analysis. Heatmaps were generated using the web-based tool Morpheus (https://software.broadinstitute.org/morpheus), and KEGG pathway enrichment analyses were performed using ShinyGO 0.85.1. Datasets are available at GSEXXX.

Multiplexed immunofluorescence. Multiplexed immunofluorescence was performed on the Comet^{TM} instrument (Lunaphore) on 5-µm paraffin-embedded non-tumour, HCC, and tumouroid sections from APC$^{\Delta hep}$ model in a 12x12 mm chamber. Slides underwent deparaffinization followed by heat-induced epitope retrieval in alkaline buffer pH 9.0 at temperature reaching 102°C, followed by controlled cooling prior to subsequent staining steps. Tissues were submitted to 16 cycles of antibody incubation/elution/image acquisition. One or two primary antibodies were added for 8 min and one or two adhoc secondary antibodies for 4 min. Used antibodies are described in **Table S2**. The fields of view were saved and the background was subtracted using the HORIZON software (Lunaphore).

Statistical analysis. Differences between two sample groups were assessed using a Mann-Whitney test. For comparisons involving more than two groups, Kruskal-Wallis test was performed. A p-value < 0.05 was considered statistically significant.

bioRxiv preprint doi: https://doi.org/10.64898/2026.04.01.715868; this version posted April 3, 2026. The copyright holder for this preprint (which was not certified by peer review) is the author/funder. All rights reserved. No reuse allowed without permission.

Results

Generation of liver organoids from Apc$^{\Delta Hep}$ mice using ClinoStar® system

For many years, 2D culture of human and murine hepatocytes on collagen matrix has been the gold standard method. However, the rapid cell dedifferentiation and cell mortality associated with this culture method have called it into question (32). Accordingly, 2D culture impacted identity of APC^{KO} hepatocytes isolated from *Apc$^{lox/lox}$/TTR-Cre^{ERT2}* mice injected with a high dose of tamoxifen (**Fig.1A**). Freshly isolated APC^{KO} hepatocytes overexpressed three major and direct β-catenin target genes, *Glul* encoding glutamine synthetase (GS) (100-fold increase), *Axin2* (100-fold increase) and *Lgr5* (30-fold increase) compared to wild-type (WT) hepatocytes isolated from *Apc$^{lox/lox}$* mice injected with tamoxifen (**Fig.1B**). After 24 hours in 2D culture, *Glul*, *Axin2* and *Lgr5* were still overexpressed in APC^{KO} hepatocytes compared to WT hepatocytes, but their fold change was lower than that observed in freshly isolated APC^{KO} hepatocytes (20-, 50-, and 0.5-fold increase, respectively). Thus, the maintenance of β-catenin-activated hepatocyte identity is rapidly altered by 2D monoculture.

We therefore decided to switch to 3D culture of APC^{KO} hepatocytes together with NPC (immune, mesenchymal and endothelial cells) (**Fig.1C**). To this aim, a 2:1 ratio of Apc^{KO} hepatocytes/NPC were seeded in a ClinoReactor and cultured during eight days in a ClinoStar®. As a comparison, Apc$^{\Delta Hep}$ organoids were also produced by static culture on ULA plates (**Fig.1C**). By preventing cell adhesion to the plastic dish, ULA plates promote the spontaneous aggregation of cells into spheroids (33). A major limitation of this technique is the formation of a necrotic core due to poor diffusion of nutrients and oxygen (34). After eight days of culture in the ClinoStar®, APC^{KO} hepatocytes mixed with NPC formed around 40 well-individualized organoids of

bioRxiv preprint doi: https://doi.org/10.64898/2026.04.01.715868; this version posted April 3, 2026. The copyright holder for this preprint (which was not certified by peer review) is the author/funder. All rights reserved. No reuse allowed without permission.

uniform area per clinoreactor (**Fig.1D-E**). High inter-experimental reproducibility was obtained with the ClinoStar® system regarding organoid area and number. Organoids also formed systematically in each well of the ULA plates, but they were smaller than those generated with the ClinoStar® (**Fig.1D-E**). After 16 days in culture, 100% of liver organoids retained a compact, and rounded morphology in the ClinoStar®, unlike those cultured in ULA plates, 62% of which showed structural loosening and tended to be smaller (**Fig.1D, E**). These findings highlight the advantage of dynamic rotational culture in preserving organoid structural integrity and probably viability and proliferation features over extended periods.

At the molecular level, *Glul* mRNA expression was similar between $Apc^{\Delta Hep}$ organoids generated in the ClinoStar® after eight days in culture and freshly isolated APC^{KO} hepatocytes, whereas *Glul* expression was significantly reduced in $Apc^{\Delta Hep}$ organoids generated in ULA plates (**Fig.1F**). Histology and IHC analyses were then performed to better characterize $Apc^{\Delta Hep}$ organoid structures obtained from both conditions (**Fig.2A**). After staining with HE, numerous cells lacking nucleus were observed in the core of organoids obtained from the ULA plates suggesting cell death, whereas such cellular entities were not observed in the organoids from the ClinoStar® (**Fig.2B**). Consistently, the detection of cleaved caspase-3 revealed strong staining in organoids generated with ULA plates but not with the ClinoStar® (**Fig.2B-C**), indicating that the ClinoStar® device limits cell death in $Apc^{\Delta Hep}$ organoids. $Apc^{\Delta Hep}$ organoids produced in the ClinoStar® also showed homogeneous GS labelling as well as membrane, cytoplasmic and nuclear staining of β-catenin. TUNEL assay revealed an increased number of positive cells in organoids generated in ULA plates compared to those generated in the ClinoStar®, confirming enhanced cell apoptosis in ULA plates (**Fig.2D**). Importantly, NPC were detected within $Apc^{\Delta Hep}$ organoids. Thus,

bioRxiv preprint doi: https://doi.org/10.64898/2026.04.01.715868; this version posted April 3, 2026. The copyright holder for this preprint (which was not certified by peer review) is the author/funder. All rights reserved. No reuse allowed without permission.

macrophages and endothelial cells were evidenced using F4/80 and CD146 immunostaining, respectively (**Fig.2B-C**). Finally, higher level of cell proliferation (KI67 staining) was observed in $Apc^{\Delta Hep}$ organoids produced in the ClinoStar® compared to ULA plates (**Fig.2B-C**). The presence of dead cells in $Apc^{\Delta Hep}$ organoids obtained using ULA plates had an impact on the quality of IHC, which was either difficult to detect (GS, cytoplasmic and nuclear β-catenin) or accompanied by significant background noise and non-specific staining (KI67, F4/80, CD146) (**Fig.2B**). Overall, these data indicate that the ClinoStar® system offers favourable conditions for the production of β-catenin-activated liver organoids by allowing the maintenance of different cell populations in the absence of cell death.

Generation of liver tumouroids from $Apc^{\Delta Hep}$ and $\beta cat^{\Delta ex3}$ mouse tumours using ClinoStar® system

These data led us to investigate whether ClinoStar® system could be also useful for generating β-catenin-activated tumouroids. To this end, $Apc^{lox/lox}$ mice were injected with an adenovirus encoding Cre recombinase (AdCre) and followed by ultrasounds for tumour development during several months. Once tumours had been detected, they were harvested, dissociated mechanically and enzymatically, and seeded in bioreactors (**Fig.3A**). Two types of tumours were obtained from these mice, either well-differentiated $APC^{\Delta hep}$ HCC (n=5) or undifferentiated $APC^{\Delta hep}$ HB-like tumours (n=4).

After eight days of culture in the ClinoStar®, we observed that tumour cells and NPC isolated from both HCC and HB-like tumours formed 3D structures, with approximately 30–40 tumouroids per culture and diameters ranging from 250 to 300 µm. These 3D structures reproduced the structural and cellular complexity of their native tumour tissue. Thus, $APC^{\Delta hep}$ HCC tumouroids retained β-catenin pathway

bioRxiv preprint doi: https://doi.org/10.64898/2026.04.01.715868; this version posted April 3, 2026. The copyright holder for this preprint (which was not certified by peer review) is the author/funder. All rights reserved. No reuse allowed without permission.

activation, evidenced by strong cytoplasmic staining of GS and membrane, cytoplasmic and nuclear staining of β-catenin (**Fig.3B**). As expected, HB-like tumouroids show less intense GS staining together with strong vimentin staining, underlying their mesenchymal status (**Fig.4**). No cell death (cleaved caspase-3 staining) was detected in the core of tumouroids, regardless of the type of the tumour of origin, while proliferative hepatocytes (KI67 staining) were detected throughout these 3D structures. As observed in the preneoplastic organoids (**Fig.2**), F4/80 and CD146 staining revealed the presence of macrophages and endothelial cells, respectively. Besides conventional IHC with chromogenic detection, tumouroids from APC$^{\Delta Hep}$ HCC were also analyzed using a high-throughput automated multiplex immunofluorescence staining platform which relies on high-pressure microfluidic circuits. As shown in **Fig.S2**, the detection of proteins specific for the different cell subtypes was clearly evidenced within APC$^{\Delta hep}$ HCC tumouroids.

We confirmed these data with βcat$^{\Delta ex3}$ HCC which is equivalent to APC$^{\Delta Hep}$ HCC at the transcriptomic level (17). Tumouroids derived from βcat$^{\Delta ex3}$ HCC retained the histological architecture from their original tumour (**Fig.S3**). Altogether, these data suggest that the dynamic culture in the ClinoStar® is efficient to generate tumouroids from both murine β-catenin-activated HCC and HB-like tumours, which preserve intra-tumoural cellular heterogeneity.

APC$^{\Delta hep}$ tumouroids cultured in the ClinoStar® maintain the transcriptome of the tumour of origin

We further performed RNA-seq to characterize APC$^{\Delta hep}$ HCC (n=5) and HB tumouroids (n=4) compared to their native tumours and adjacent non-tumour tissues. Principal component analysis (PCA) indicated that each tumouroid was perfectly clustered with

bioRxiv preprint doi: https://doi.org/10.64898/2026.04.01.715868; this version posted April 3, 2026. The copyright holder for this preprint (which was not certified by peer review) is the author/funder. All rights reserved. No reuse allowed without permission.

its tumour of origin, while non-tumour tissues were clearly separated into a tight cluster (**Fig.5A** for HCC and **Fig.6A** for HB). Samples from HCC#1/tumouroid#1 appeared to be outliers. The data for HCC#1 showed that it was a larger tumour (12 mm compared with 7-8 mm for the others), exhibiting signs of apoptosis (data not shown). Differentially expressed genes were then analyzed by MA plots, which also revealed tiny differences between each tumouroid and its tumour of origin (**Fig.5B** for HCC and **Fig.6B** for HB). Only *Fam177a2* and *2810047C21Rik* (a RIKEN-annotated mouse gene with unknown function) were significantly upregulated in HB-like tumouroids compared with tumours (**Fig.6B**). We then examined the expression pattern of genes specific to each type of tumouroids compared to non-tumour liver tissue (**Fig.5C** and **Fig.6C**; samples HCC#1/tumouroid#1 were excluded from this analysis). As previously described in APC$^{\Delta hep}$ HCC (30, 35–37), HCC tumouroids expressed high levels of *Ctnnb1* targets genes (both canonical and liver specific genes), genes involved in glutamine, bile and drug metabolisms, inflammation, redox signaling as well as low levels of genes involved in amino acid catabolism (**Fig.5C**). Similar to the APC$^{\Delta hep}$ HB-like tumours (17, 38), HB-like tumouroids expressed high levels of canonical *Ctnnb1* target genes as well as Apc$^{\Delta hep}$ embryonic liver genes, mesenchymal markers and Hippo signature (**Fig.6C**). Transcripts encoding vascular markers such as *Mcam*/Cd146 were also significantly induced in both Apc$^{\Delta hep}$ HCC and HB-like, confirming our observations in IHC (**Fig.3B** and **Fig.4**). KEGG pathway enrichment analysis was also performed between tumouroids and their non-tumoural related samples. In HCC-derived tumouroids, some of the pathways showing the highest enrichment scores were related to cell cycle and xenobiotic and gluthatione metabolisms (**Fig.5D**) while pathways related to amino acid metabolism were among the most downregulated (**Fig.5E**). Several pathways related to mitosis and cell division

bioRxiv preprint doi: https://doi.org/10.64898/2026.04.01.715868; this version posted April 3, 2026. The copyright holder for this preprint (which was not certified by peer review) is the author/funder. All rights reserved. No reuse allowed without permission.

showed high enrichment scores in HB-derived tumouroids (**Fig.6D**) while several pathways related to lipid metabolism were downregulated (**Fig.6E**). This analysis confirms substantial pathway-level differences between tumouroids derived from HCC and HB and their non-tumoural tissues, which are consistent with the biological characteristics of the native tumours: a more metabolic phenotype for HCC and a more proliferative phenotype for HB-like tumours. Collectively, these data demonstrate that our protocol and culture conditions generate murine HCC and HB-like tumouroids which recapitulate the complexity and oncogenic programs of tumours of origins.

WNTinib suppresses proliferation and promotes apoptotic responses in β-catenin-activated organoids and tumouroids

To investigate whether organoids and tumouroids generated in the ClinoStar® could be new relevant preclinical tools for drug screening, we treated both $APC^{\Delta hep}$ organoids and $\beta cat^{\Delta ex3}$ tumouroids with WNTinib, a recently identified multi-kinase inhibitor which demonstrated efficiency against human HCC and HB cells with *CTNNB1* activating mutations (39, 40). Once $APC^{\Delta hep}$ organoids had formed after eight days of culture in the ClinoStar®, 1 µM WNTinib was added for five additional days. As observed in **Fig.7A** and **Fig.7B**, WNTinib induced marked structural and molecular changes. HE staining showed a disorganized structure with cells without nucleus within the core of the treated organoids compared to untreated ones. GS immunostaining was less intense under treatment with WNTinib, while cleaved caspase-3 was detected within treated organoids only. TUNEL assay revealed increased number of positive cells in WNTinib-treated organoids, confirming enhanced cell apoptosis (**Fig.S3,** *upper panel*). Proliferation was also markedly reduced in treated organoids as evidenced with KI67 immunostaining (**Fig.7A-B**). The repression of the β-catenin signalling pathway,

bioRxiv preprint doi: https://doi.org/10.64898/2026.04.01.715868; this version posted April 3, 2026. The copyright holder for this preprint (which was not certified by peer review) is the author/funder. All rights reserved. No reuse allowed without permission.

associated with downregulation of *Glul* and *Axin2* mRNA as well as the induction of apoptosis, evidenced by the induction of the pro-apoptotic *Noxa* mRNA and the downregulation of anti-apoptotic *Bcl2l1* mRNA, were also demonstrated by RT-PCR in WNTinib-treated APC$^{\Delta hep}$ organoids (**Fig.7C**). We also investigated whether βcat$^{\Delta ex3}$ HCC-derived tumouroids were sensitive to WNTinib. After eight days of culture, HCC tumouroids were treated with 5 µM WNTinib for five additional days in the ClinoStar®. WNTinib induced the appearance of cells without nucleus within tumouroid core which was associated with an apoptotic program revealed by increased caspase-3 cleavage (**Fig. 7D**) and TUNEL labelling (**Fig.S3,** *lower panel*) as well as increased *Noxa* and decreased *Bcl2l1* mRNA levels (**Fig.7F**). WNTinib also reduced the numbers of Ki67+ cells (**Fig.7D-E**). These data unveil both preneoplastic organoids and tumouroids as new powerful preclinical models for drug screening.

bioRxiv preprint doi: https://doi.org/10.64898/2026.04.01.715868; this version posted April 3, 2026. The copyright holder for this preprint (which was not certified by peer review) is the author/funder. All rights reserved. No reuse allowed without permission.

Discussion

In the present study, we successfully established murine preneoplastic organoids from livers with hepatospecific β-catenin overactivation as well as tumouroids from β-catenin-activated well differentiated HCC and poorly differentiated HB-like tumours. IHC and gene expression analyses reveal that these organoids and tumouroids retain their histological architecture and the expression patterns of their tumour they derived from. This success is based on the use of a vertical rotary bioreactor which utilizes gentle rotational dynamics to achieve near-microgravity conditions, thus reducing shear stress while maintaining optimal nutrient and oxygen distribution (26). The morphological homogeneity and size reproducibility of liver organoids and tumouroids cultured in the ClinoStar® system are consistent with the findings of recent studies using this technology to establish brain organoids (41) and lung tumouroids (42). Moreover, organoids and tumouroids generated from mouse livers and tumours with β-catenin activation, respectively, showed very low levels of cleaved caspase-3, particularly in their core, indicating that dynamic culture limits hypoxia and the subsequent apoptotic cell death. The protocol we have developed is relatively simple, relies on commercially available cell culture media, and does not require a preliminary step of aggregating dissociated cells in hydrogel or micropattern plates, as has been previously reported for other tissues and cell types (43). Furthermore, this protocol does not involve the addition of extracellular matrix, which increases reproducibility across experiments due to the absence of undefined factors associated with matrix-based products. Interestingly, this culture method allows hepatic organoids and tumouroids to maintain cellular diversity for at least 8 days, as highly differentiated and undifferentiated tumour hepatocytes, macrophages and endothelial cells were detected within these structures. This shows that this type of culture helps preserve a

bioRxiv preprint doi: https://doi.org/10.64898/2026.04.01.715868; this version posted April 3, 2026. The copyright holder for this preprint (which was not certified by peer review) is the author/funder. All rights reserved. No reuse allowed without permission.

certain degree of tumour complexity. While the ClinoStar® device has been described previously as capable of generating spheroids from the HepG2 liver cancer cell line (28, 44), our study is the first to report its use for the formation of organoids and tumouroids from preneoplastic hepatocytes and liver tumours. The therapeutic management of primary liver tumours, particularly tumours activated for the β-catenin pathway, still requires further research. Thus, HCCs with a β-catenin mutated pathway, which account for up to 40% of HCCs, exhibit immune exclusion (with regard to T lymphocyte infiltration) and, when inoperable, are more refractory to standard treatments that combine immunotherapies (8, 45–47). The treatment for HB consists of cisplatin-based chemotherapy before and after surgery (14). However, resistance to chemotherapy is observed in metastatic or recurrent cases and the toxicity of chemotherapy can be a major concern in young patients (14). It is therefore essential to identify other vulnerabilities, overcome chemoresistance and develop therapies with low toxicities to improve HCC and HB patient outcomes.

2D and 3D cultures of human HCC and HB cell lines have long been used as a reference for *in vitro* drug screening, but due to their clonal and single-cell type nature, these models cannot recapitulate tumour heterogeneity, which may limit data translational value. Patient-derived xenografts have proved to be useful models for human HCC and HB (23, 48, 49) because they retain histology and gene expression from their tumour of origin. However, the establishment of mouse cohorts with PDXs is time-consuming, not always successful (the engraftment efficiency may be low), expensive, and not suitable for large-scale drug sensitivity testing because it does not fit within the framework of human animal research. Therefore, tumouroid cultures represent an alternative resource for drug discovery to liver cancer PDXs. The Meritxell Huch group pioneered this field by developing matrix-embedded tumouroids from

bioRxiv preprint doi: https://doi.org/10.64898/2026.04.01.715868; this version posted April 3, 2026. The copyright holder for this preprint (which was not certified by peer review) is the author/funder. All rights reserved. No reuse allowed without permission.

human HCC and cholangiocarcinoma (48). They showed that their tumouroids are reliable *in vitro* cancer models, recapitulating the main features of the different subtypes of HCC and cholangiocarcinoma analyzed. Since then, this technology has been used by other groups to develop tumouroids from different mouse models of liver carcinogenesis (44, 49).

Within this framework, our study provides proof of concept that dynamic culture in a ClinoStar® represents a suitable approach for generating tumouroids applicable to HCC and HB modeling and drug screening. From a small fragment of tumour, we were able to produce dozens of tumouroids from murine HCC and HB that are highly similar in terms of shape, size, and cellular content and mirror the tumour of origin. The mouse models used in our study have demonstrated their clinical relevance in several studies. Thus, $Apc^{\Delta Hep}$ mice with activation of the β-catenin pathway throughout the hepatic lobules, from which the spheroids described herein were derived, have proven useful for characterizing the early stages of constitutive activation of the β-catenin pathway in hepatocytes (24). $Apc^{\Delta Hep}$ and $\beta cat^{\Delta ex3}$ mice exhibiting focal activation of the β-catenin pathway in the liver develop differentiated HCC and HB-like mesenchymal tumours that mimic human tumours at the histological and transcriptional levels (26). Murine HCC also exhibit metabolic traits such as glutamine anabolism and choline addiction (18), as well as responses to oxydative stress that mimic those observed in human HCC (35). Our new models should significantly reduce the number of mice used in pre-selection and evaluation tests for new therapeutic agents. In order to prove the concept that the murine tumouroids we generated from HCC would be useful for drug screening, we tested their sensitivity to WNTinib. WNTinib is a multikinase inhibitor which has been recently identified as a transcriptional repressor of mutant β-catenin and it has been evaluated in human liver

bioRxiv preprint doi: https://doi.org/10.64898/2026.04.01.715868; this version posted April 3, 2026. The copyright holder for this preprint (which was not certified by peer review) is the author/funder. All rights reserved. No reuse allowed without permission.

cancer cell lines cultured in 2D and mouse- and patient-derived HCC and HB tumouroids cultured in Matrigel (39, 40, 44). In our dynamic culture, WNTinib potently inhibited proliferation and induced apoptosis in murine HCC tumouroids, consistent with its previously identified modes of action. This opens the way to test other drugs in our HCC and HB-like models.

In conclusion, we provide a new methodology for the generation of murine tumouroids from β-catenin-driven HCC and HB. These tumouroids represent valuable resources which should be useful tools for both basic cancer research and the development of precision medicine due to their translational and ethical advantages, especially their potential to reduce animal experimentation. Beyond these models, this methodology could be extended to tumours derived from other murine models of liver cancer, thereby broadening its applicability for studying diverse oncogenic contexts. Moreover, the compatibility of this approach with the generation of tumouroids from human liver tumour fragments is currently being investigated, which could further enhance its translational potential.

bioRxiv preprint doi: https://doi.org/10.64898/2026.04.01.715868; this version posted April 3, 2026. The copyright holder for this preprint (which was not certified by peer review) is the author/funder. All rights reserved. No reuse allowed without permission.

Acknowledgements: We are grateful to CRC core facilities (INSERM UMRS_1138, Sorbonne Université, Université Paris Cité) and their team members for animal care and breeding (CFE, Mrs Sonia Prince), genotyping (CGB, Mrs Hermine Kakanakou), and cell imaging (CHICS, Dr Christophe Klein). We warmly thank the Institut Cochin's core facilities (INSERM U1016, CNRS UMR8104, Université Paris Cité) and their team members for animal care and breeding (Moust'IC, Mr Marcio Do-Cruzeiro), liver ultrasonography (PIV, Dr Gilles Renault) and transcriptomic analysis (Genom'IC, Dr Franck Letourneur). Dr Véronique Blouin (CAPACITES, INSERM UMR1089, Université de Nantes, France) is thanked for recombinant AAV8 production. Dr Ronan Le Bouffant and Dr Helle Sedighi Frandsen are thanked for critical reading of the manuscript.

bioRxiv preprint doi: https://doi.org/10.64898/2026.04.01.715868; this version posted April 3, 2026. The copyright holder for this preprint (which was not certified by peer review) is the author/funder. All rights reserved. No reuse allowed without permission.

Legends to Figures

Fig.1 Generation of liver organoids from Apc$^{\Delta Hep}$ mice in ULA plates and a ClinoStar®-based 3D culture system.

(A) Schematic illustration of the experimental design for 2D culture of APC^{KO} hepatocytes (Created with BioRender.com). **(B)** Expression of *Glul*, *Axin2* and *Lgr5* transcripts assessed by RT-qPCR (n = 5) in freshly isolated APC^{KO} hepatocytes or after 24 h in 2D culture normalized to WT fresh pellets. **(C)** Schematic illustration of the experimental design for 3D culture of organoids (Created with BioRender.com) **(D)** Representative brightfield images of liver APC$^{\Delta Hep}$ organoids acquired 8 or 16 days after cell plating in ULA plates or in the ClinoStar®. **(E)** Quantification of the organoid integrity area (mm^2) at day 8 and 16 after plating in ULA plates or in the ClinoStar®. **(F)** Expression of *Glul* transcripts assessed by RT-qPCR (n = 5) under the different culture conditions. All bar graphs represent mean values ± SD, with individual dots corresponding to independent samples. For comparisons involving more than two groups, Kruskal-Wallis test was performed.

Fig.2 Beyond ULA plates: 3D culture in a ClinoStar® improves the development of APC$^{\Delta Hep}$ liver organoids

(A) Schematic illustration of the spheroid inclusion protocol (Created with BioRender.com). **(B)** Representative HE staining and immunostaining for cleaved capase-3, GS, β-catenin, KI67, F4/80 and CD146 in APC$^{\Delta Hep}$ organoids generated after 8 days in ULA plates (*left panel*) or in the ClinoStar® (*right panel*). The black arrows indicate nuclei positively stained for KI67. **(C)** Quantitative analysis of KI67,

bioRxiv preprint doi: https://doi.org/10.64898/2026.04.01.715868; this version posted April 3, 2026. The copyright holder for this preprint (which was not certified by peer review) is the author/funder. All rights reserved. No reuse allowed without permission.

cleaved caspase-3, F4/80 and CD146 positive cells in organoids cultured in ULA plates or ClinoStar® (n = 6). **(D)** Representative images of apoptotic cells detected by TUNEL staining (red), with nuclei counterstained with DAPI (blue) in organoids cultured during 8 days in ULA plates (*left panel*) or in the ClinoStar® (*right panel*). All bar graphs represent mean values ± SD, with individual dots corresponding to independent samples. Differences between two sample groups were assessed using a Mann-Whitney test.

Fig.3 Culture in the ClinoStar® generates and preserves Apc$^{\Delta Hep}$ HCC tumouroids

(A) Schematic illustration of the experimental design for 3D culture (Created with BioRender.com). **(B)** Representative HE staining and immunostaining for cleaved capase-3, GS, β-catenin, KI67, F4/80 and CD146 in tumouroids formed 8 days after plating in the ClinoStar®, compared to their native HCC. The black arrows indicate nuclei positively stained for KI67.

Fig.4 Culture in the ClinoStar® generates and preserves Apc$^{\Delta Hep}$ HB-like tumouroids

Representative HE staining and immunostaining for cleaved capase-3, GS, β-catenin, KI67, F4/80 and CD146 in tumouroids formed 8 days after plating in the ClinoStar® compared to their native HB-like tumours. The black arrows indicate nuclei positively stained for KI67.

Fig.5 Culture in the ClinoStar® maintains the transcriptomic programs of Apc$^{\Delta Hep}$ HCC tumouroids

bioRxiv preprint doi: https://doi.org/10.64898/2026.04.01.715868; this version posted April 3, 2026. The copyright holder for this preprint (which was not certified by peer review) is the author/funder. All rights reserved. No reuse allowed without permission.

(A) PCA of normalized gene expression profiles from tumouroids, HCC and adjacent non-tumoural livers. **(B)** MA plot showing gene expression between each tumouroid and its corresponding HCC. Each dot represents a gene, plotted as Log2 fold change versus the mean of normalized counts across all samples. Significantly upregulated genes are shown in orange, downregulated genes in blue, and non-significant genes in grey. **(C)** Heatmap of differentially expressed genes between tumouroids, HCC, and adjacent non-tumoural livers. Unsupervised hierarchical clustering was performed on samples. **(D)** KEGG pathway enrichment analysis of genes significantly upregulated in tumouroids compared to adjacent non-tumoural livers. **(E)** KEGG pathway enrichment analysis of genes significantly downregulated in tumouroids compared to adjacent non-tumoural livers.

Fig.6 Culture in the ClinoStar® maintains the transcriptomic programs of Apc$^{\Delta Hep}$ HB-like tumouroids

(A) PCA of normalized gene expression profiles from tumouroids, HB-like tumours and adjacent non-tumoural livers. **(B)** MA plot showing gene expression between each tumouroid and its corresponding HB-like tumour. Each dot represents a gene, plotted as Log2 fold change versus the mean of normalized counts across all samples. Significantly upregulated genes are shown in orange, downregulated genes in blue, and non-significant genes in grey. **(C)** Heatmap of differentially expressed genes between tumouroids, HB-like tumours and adjacent non-tumoural livers. Unsupervised hierarchical clustering was performed on both genes and samples. **(D)** KEGG pathway enrichment analysis of genes significantly upregulated in tumouroids compared with adjacent non-tumoural livers. **(E)** KEGG pathway enrichment analysis of genes significantly downregulated in tumouroids compared with adjacent non-tumoural livers.

bioRxiv preprint doi: https://doi.org/10.64898/2026.04.01.715868; this version posted April 3, 2026. The copyright holder for this preprint (which was not certified by peer review) is the author/funder. All rights reserved. No reuse allowed without permission.

Fig.7 WNTinib induces apoptosis and impairs proliferation in Apc$^{\Delta Hep}$ liver organoids and βcat$^{\Delta ex3}$ HCC tumouroids

(A) Representative HE staining and immunostaining for GS, cleaved caspase-3 and KI67 in Apc$^{\Delta Hep}$ organoids formed 8 days after plating in the ClinoStar® and treated with WNTinib at 1 µM or DMSO for 5 days. The black arrows indicate nuclei positively stained for KI67. **(B)** Quantification of cleaved caspase-3 and KI67 positive cells in DMSO- and WNTinib-treated organoids (n = 5). **(C)** Expression of *Noxa*, *Bcl2l1*, *Glul* and *Axin2* transcripts evaluated by RT-qPCR (n = 5) in WNTinib- and DMSO-treated organoids. **(D)** Representative hematoxylin–eosin staining and immunostaining for GS, cleaved caspase-3 and KI67 in βcat$^{\Delta ex3}$ HCC tumouroids formed 8 days after plating in the ClinoStar® and treated with WNTinib at 5 µM or DMSO for 5 days. The black arrows indicate nuclei positively stained for KI67. **(E)** Quantification of cleaved caspase-3 and KI67 positive cells in DMSO- and WNTinib-treated βcat$^{\Delta ex3}$ HCC tumouroids (n = 3). **(F)** Expression of *Noxa* and *Bcl2l1* transcripts evaluated by RT-qPCR (n = 3) in DMSO- and WNTinib-treated βcat$^{\Delta ex3}$ tumouroids. All bar graphs represent mean values ± SD, with individual dots corresponding to independent samples. Differences between two sample groups were assessed using a Mann–Whitney test.

bioRxiv preprint doi: https://doi.org/10.64898/2026.04.01.715868; this version posted April 3, 2026. The copyright holder for this preprint (which was not certified by peer review) is the author/funder. All rights reserved. No reuse allowed without permission.

List of abbreviations: AAV8, adeno-associated virus serotype 8; AdCre, adenovirus encoding Cre recombinase; BSA, bovine serum albumin; FBS, fetal bovine serum; GS, glutamine synthetase; HB, hepatoblastoma; HE, hematoxylin and eosin; IHC, immunohistochemistry; NPC, non-parenchymal cells; PCA, principal component analysis; PDX, patient-derived xenograft; 2D, two dimensional; 3D, three dimensional; ULA, ultra-low attachment; WT, wild-type.

bioRxiv preprint doi: https://doi.org/10.64898/2026.04.01.715868; this version posted April 3, 2026. The copyright holder for this preprint (which was not certified by peer review) is the author/funder. All rights reserved. No reuse allowed without permission.

References

1. Vogel A, Meyer T, Sapisochin G, Salem R, Saborowski A. Hepatocellular carcinoma. The Lancet. 2022; 400(10360):1345–62.

2. Jeong SU, Kang HJ. Recent updates on the classification of hepatoblastoma according to the International Pediatric Liver Tumors Consensus. J Liver Cancer. 2022; 22(1):23–9.

3. Xu C, Xu Z, Zhang Y, Evert M, Calvisi DF, Chen X. β-Catenin signaling in hepatocellular carcinoma. J Clin Invest. 2022; 132(4):e154515.

4. Lehrich BM, Monga SP. WNT–β-catenin signalling in hepatocellular carcinoma: from bench to clinical trials. Nat Rev Gastroenterol Hepatol. Nature Publishing Group; 2025; 1–18.

5. Harding JJ, Nandakumar S, Armenia J, Khalil DN, Albano M, Ly M, et al. Prospective Genotyping of Hepatocellular Carcinoma: Clinical Implications of Next-Generation Sequencing for Matching Patients to Targeted and Immune Therapies. Clin Cancer Res Off J Am Assoc Cancer Res. 2019; 25(7):2116–26.

6. Luke JJ, Bao R, Sweis RF, Spranger S, Gajewski TF. WNT/β-catenin Pathway Activation Correlates with Immune Exclusion across Human Cancers. Clin Cancer Res Off J Am Assoc Cancer Res. 2019; 25(10):3074–83.

7. Pinyol R, Montal R, Bassaganyas L, Sia D, Takayama T, Chau G-Y, et al. Molecular predictors of prevention of recurrence in HCC with sorafenib as adjuvant treatment and prognostic factors in the phase 3 STORM trial. Gut. 2019; 68(6):1065–75.

8. Ruiz de Galarreta M, Bresnahan E, Molina-Sánchez P, Lindblad KE, Maier B, Sia D, et al. β-Catenin Activation Promotes Immune Escape and Resistance to Anti-PD-1 Therapy in Hepatocellular Carcinoma. Cancer Discov. 2019; 9(8):1124–41.

9. Hooks KB, Audoux J, Fazli H, Lesjean S, Ernault T, Dugot-Senant N, et al. New insights into diagnosis and therapeutic options for proliferative hepatoblastoma. Hepatology. Baltimore, Md.; 2018; 68(1):89–102.

10. Cairo S, Armengol C, De Reyniès A, Wei Y, Thomas E, Renard C-A, et al. Hepatic stem-like phenotype and interplay of Wnt/beta-catenin and Myc signaling in aggressive childhood liver cancer. Cancer Cell. 2008; 14(6):471–84.

11. Hirsch TZ, Pilet J, Morcrette G, Roehrig A, Monteiro BJE, Molina L, et al. Integrated Genomic Analysis Identifies Driver Genes and Cisplatin-Resistant Progenitor Phenotype in Pediatric Liver Cancer. Cancer Discov. 2021; 11(10):2524–43.

12. Nagae G, Yamamoto S, Fujita M, Fujita T, Nonaka A, Umeda T, et al. Genetic and epigenetic basis of hepatoblastoma diversity. Nat Commun. 2021; 12(1):5423.

bioRxiv preprint doi: https://doi.org/10.64898/2026.04.01.715868; this version posted April 3, 2026. The copyright holder for this preprint (which was not certified by peer review) is the author/funder. All rights reserved. No reuse allowed without permission.

13. Sumazin P, Chen Y, Treviño LR, Sarabia SF, Hampton OA, Patel K, et al. Genomic analysis of hepatoblastoma identifies distinct molecular and prognostic subgroups. Hepatology. Baltimore, Md.; 2017; 65(1):104–21.

14. Yang T, Whitlock RS, Vasudevan SA. Surgical Management of Hepatoblastoma and Recent Advances. Cancers. 2019; 11(12):1944.

15. Bissig-Choisat B, Kettlun-Leyton C, Legras XD, Zorman B, Barzi M, Chen LL, et al. Novel patient-derived xenograft and cell line models for therapeutic testing of pediatric liver cancer. J Hepatol. 2016; 65(2):325–33.

16. Colnot S, Decaens T, Niwa-Kawakita M, Godard C, Hamard G, Kahn A, et al. Liver-targeted disruption of Apc in mice activates beta-catenin signaling and leads to hepatocellular carcinomas. Proc Natl Acad Sci U S A. 2004; 101(49):17216–21.

17. Loesch R, Caruso S, Paradis V, Godard C, Gougelet A, Renault G, et al. Deleting the β-catenin degradation domain in mouse hepatocytes drives hepatocellular carcinoma or hepatoblastoma-like tumor growth. J Hepatol. 2022; 77(2):424–35.

18. Gougelet A, Sartor C, Senni N, Calderaro J, Fartoux L, Lequoy M, et al. Hepatocellular Carcinomas With Mutational Activation of Beta-Catenin Require Choline and Can Be Detected by Positron Emission Tomography. Gastroenterology. 2019; 157(3):807–22.

19. Gougelet A, Sartor C, Bachelot L, Godard C, Marchiol C, Renault G, et al. Antitumour activity of an inhibitor of miR-34a in liver cancer with β-catenin-mutations. Gut. 2016; 65(6):1024–34.

20. Sanceau J, Poupel L, Joubel C, Lagoutte I, Caruso S, Pinto S, et al. *DLK1/DIO3* locus upregulation by a β-catenin-dependent enhancer drives cell proliferation and liver tumorigenesis. Mol Ther. 2024; 32(4):1125–43.

21. Zhang G, Liang Q, Wu Y, Wang Y. Insights on the differences between two- and three-dimensional culture systems in tumor models (Review). Int J Mol Med. 2025; 56(5):185.

22. Abuwatfa WH, Pitt WG, Husseini GA. Scaffold-based 3D cell culture models in cancer research. J Biomed Sci. 2024; 31(1):7.

23. Urzì O, Gasparro R, Costanzo E, De Luca A, Giavaresi G, Fontana S, et al. Three-Dimensional Cell Cultures: The Bridge between In Vitro and In Vivo Models. Int J Mol Sci. 2023; 24(15):12046.

24. Jubelin C, Muñoz-Garcia J, Griscom L, Cochonneau D, Ollivier E, Heymann M-F, et al. Three-dimensional in vitro culture models in oncology research. Cell Biosci. 2022; 12(1):155.

25. Lee S-Y, Koo I-S, Hwang HJ, Lee DW. In Vitro three-dimensional (3D) cell culture tools for spheroid and organoid models. SLAS Discov Adv Life Sci R D. 2023; 28(4):119–37.

bioRxiv preprint doi: https://doi.org/10.64898/2026.04.01.715868; this version posted April 3, 2026. The copyright holder for this preprint (which was not certified by peer review) is the author/funder. All rights reserved. No reuse allowed without permission.

26. Wrzesinski K, Fey SJ. Metabolic Reprogramming and the Recovery of Physiological Functionality in 3D Cultures in Micro-Bioreactors. Bioengineering. 2018; 5(1):22.

27. Stransky S, Cutler R, Aguilan J, Nieves E, Sidoli S. Investigation of reversible histone acetylation and dynamics in gene expression regulation using 3D liver spheroid model. Epigenetics Chromatin. 2022; 15(1):35.

28. Kim C, Zhu Z, Barbazuk WB, Bacher RL, Vulpe CD. Time-course characterization of whole-transcriptome dynamics of HepG2/C3A spheroids and its toxicological implications. Toxicol Lett. 2024; 401:125–38.

29. Štampar M, Sedighi Frandsen H, Rogowska-Wrzesinska A, Wrzesinski K, Filipič M, Žegura B. Hepatocellular carcinoma (HepG2/C3A) cell-based 3D model for genotoxicity testing of chemicals. Sci Total Environ. 2021; 755(Pt 2):143255.

30. Gougelet A, Torre C, Veber P, Sartor C, Bachelot L, Denechaud P-D, et al. T-cell factor 4 and β-catenin chromatin occupancies pattern zonal liver metabolism in mice. Hepatology. Baltimore, Md.; 2014; 59(6):2344–57.

31. Bankhead P, Loughrey MB, Fernández JA, Dombrowski Y, McArt DG, Dunne PD, et al. QuPath: Open source software for digital pathology image analysis. Sci Rep. 2017; 7(1):16878.

32. Torres S, Abdullah Z, Brol MJ, Hellerbrand C, Fernandez M, Fiorotto R, et al. Recent Advances in Practical Methods for Liver Cell Biology: A Short Overview. Int J Mol Sci. 2020; 21(6):2027.

33. Kasamkattil J, Gryadunova A, Martin I, Barbero A, Schären S, Krupkova O, et al. Spheroid-Based Tissue Engineering Strategies for Regeneration of the Intervertebral Disc. Int J Mol Sci [Internet]. publisher; 2022 [cited 2026 Feb 9]; 23(5). Available from: https://www.mdpi.com/1422-0067/23/5/2530.

34. Han SJ, Kwon S, Kim KS. Challenges of applying multicellular tumor spheroids in preclinical phase. Cancer Cell Int. 2021; 21(1):152.

35. Senni N, Savall M, Cabrerizo Granados D, Alves-Guerra M-C, Sartor C, Lagoutte I, et al. β-catenin-activated hepatocellular carcinomas are addicted to fatty acids. Gut. 2019; 68(2):322–34.

36. Anson M, Crain-Denoyelle A-M, Baud V, Chereau F, Gougelet A, Terris B, et al. Oncogenic β-catenin triggers an inflammatory response that determines the aggressiveness of hepatocellular carcinoma in mice. J Clin Invest. 2012; 122(2):586–99.

37. Abitbol S, Dahmani R, Coulouarn C, Ragazzon B, Mlecnik B, Senni N, et al. AXIN deficiency in human and mouse hepatocytes induces hepatocellular carcinoma in the absence of β-catenin activation. J Hepatol. 2018; 68(6):1203–13.

38. Kluiver TA, Lu Y, Schubert SA, Kraaier LJ, Ringnalda F, Lijnzaad P, et al. Divergent WNT signaling and drug sensitivity profiles within hepatoblastoma tumors and organoids. Nat Commun. Nature Publishing Group; 2024; 15(1):8576.

bioRxiv preprint doi: https://doi.org/10.64898/2026.04.01.715868; this version posted April 3, 2026. The copyright holder for this preprint (which was not certified by peer review) is the author/funder. All rights reserved. No reuse allowed without permission.

39. Balaseviciute U, Huguet-Pradell J, Abril-Fornaguera J, Gris-Oliver A, Rialdi A, Fernández-Martínez E, et al. Effective therapeutic targeting of CTNNB1-mutant hepatoblastoma with WNTinib. Mol Oncol. 2025.

40. Rialdi A, Duffy M, Scopton AP, Fonseca F, Zhao JN, Schwarz M, et al. WNTinib is a multi-kinase inhibitor with specificity against β-catenin mutant hepatocellular carcinoma. Nat Cancer. Nature Publishing Group; 2023; 4(8):1157–75.

41. Aiello G, Nemir M, Vidimova B, Ramel C, Viguie J, Ravera A, et al. Increased reproducibility of brain organoids through controlled fluid dynamics. EMBO Rep. 2025; 26(24):6209–39.

42. Donà F, Erratico S, Terracciano LM, Brascia D, Cecconi ER, Giudici VM, et al. Protocol for the establishment and characterization of lung tumoroids from surgical resection without the use of Matrigel. STAR Protoc. 2025; 6(3):103923.

43. Liu Y, Gilchrist AE, Johansson PK, Guan Y, Deras JD, Liu Y-C, et al. Engineered Hydrogels for Organoid Models of Human Nonalcoholic Fatty Liver Disease. Adv Sci. Weinheim, Baden-Wurttemberg, Germany; 2025; 12(22):e17332.

44. Kim C, Zhu Z, Tagmount A, Barbazuk WB, Bacher R, Vulpe CD. Physiologically relevant 3D CRISPR screening enhances mechanistic insight into chemical toxicity compared to 2D screening. Toxicology. 2026; 522:154422.

45. Huang Y, Peng M, Yu W, Li H. Activation of Wnt/β-catenin signaling promotes immune evasion via the β-catenin/IKZF1/CCL5 axis in hepatocellular carcinoma. Int Immunopharmacol. 2024; 138:112534.

46. Pinyol R, Sia D, Llovet JM. Immune exclusion-Wnt/CTNNB1 class predicts resistance to immunotherapies in HCC. Clin Cancer Res Off J Am Assoc Cancer Res. 2019; 25(7):2021–3.

47. Morita M, Nishida N, Aoki T, Chishina H, Takita M, Ida H, et al. Role of β-Catenin Activation in the Tumor Immune Microenvironment and Immunotherapy of Hepatocellular Carcinoma. Cancers. 2023; 15(8):2311.

48. Broutier L, Mastrogiovanni G, Verstegen MM, Francies HE, Gavarró LM, Bradshaw CR, et al. Human primary liver cancer-derived organoid cultures for disease modeling and drug screening. Nat Med. 2017; 23(12):1424–35.

49. Grattarola M, Pons N, Cannet F, Kaya M, Kaoutari AE, Morel C, et al. Establishment of a mouse hepatocellular carcinoma tumoroid panel recapitulating inter- and intra- heterogeneity for disease modelling and combinatorial drug discovery. Cell Commun Signal CCS. 2025; 23(1):410.

bioRxiv preprint doi: https://doi.org/10.64898/2026.04.01.715868; this version posted April 3, 2026. The copyright holder for this preprint (which was not certified by peer review) is the author/funder. All rights reserved. No reuse allowed without permission.

Legends to supplementary figures

Fig.S1 Expression of excised *Apc* mRNA

Percentage of *Apc* mRNA excision in freshly isolated WT and $Apc^{\Delta Hep}$ hepatocytes evaluated by RT-qPCR (n = 5). Bar graphs represent mean values ± SD, with individual dots corresponding to independent samples. Differences between two sample groups were assessed using a Mann–Whitney test.

Fig.S2 Multiplex tissue profiling of HCC-derived tumouroids

Multiplex immunofluorescence was performed using COMET™ in non-tumour, HCC and tumouroids from $Apc^{\Delta Hep}$ liver mouse. Representative COMET images showing cyclin A2 (magenta), CD146 (orange), GS (purple), F4/80 (green) and the nuclei counterstained with DAPI (blue).

Fig.S3 Histological and IHC characterization of $\beta cat^{\Delta ex3}$ tumouroids

Representative sections of HE staining and immunostaining for cleaved capase-3, GS, β-catenin, KI67, F4/80 and CD146 in $\beta\text{-}cat^{\Delta ex3}$ tumouroids formed 8 days after plating in the ClinoStar®. The black arrows indicate nuclei positively stained for KI67.

Fig.S4 TUNEL assay in $Apc^{\Delta Hep}$ liver organoids and $\beta cat^{\Delta ex3}$ HCC tumouroids

Representative images of $Apc^{\Delta Hep}$ liver organoids (*top row*) and $\beta cat^{\Delta ex3}$ HCC tumouroids (*bottom row*) cultured during 8 days in the ClinoStar® system and treated with WNTinib at 1 µM (organoids) or 5 µM (tumouroids) or with DMSO for 5 days. Apoptotic cells were detected by TUNEL staining (red), with nuclei counterstained with DAPI (blue).

bioRxiv preprint doi: https://doi.org/10.64898/2026.04.01.715868; this version posted April 3, 2026. The copyright holder for this preprint (which was not certified by peer review) is the author/funder. All rights reserved. No reuse allowed without permission.

Supplementary tables

Table S1: List of primers and probes

Name	Reference/Sequence	Supplier
Apc (total transcript)	Mm00545877	ThermoFisher Scientific
Apc (exon 14 transcript)	Mm01130462	ThermoFisher Scientific
Axin2	Mm00443610	ThermoFisher Scientific
Glul	Mm00725701	ThermoFisher Scientific
Lgr5	Mm00438890	ThermoFisher Scientific
B2m	F 5'-ACAGTTCCACCCGCCTCACATT-3' R 5'-TAGAAAGACCAGTCCTTGCTGAAG-3'	Eurogentec
Noxa	F 5'-GGAAGTCGCAAAAGAGCAGGATG-3' R 5'-CTGCCGTAAATTCACTTTGTCTCC-3'	Eurogentec
Bcl2l1	F 5'-CGACCCAGCCACCACCTCCTC-3' R 5'-TGGGGACTCAGTCCTATTCTC-3'	Eurogentec

bioRxiv preprint doi: https://doi.org/10.64898/2026.04.01.715868; this version posted April 3, 2026. The copyright holder for this preprint (which was not certified by peer review) is the author/funder. All rights reserved. No reuse allowed without permission.

Table S2: List of antibodies used in IHC and multiplex staining

Name	Supplier	Reference	Dilution	Application
Cyclin A2	Abcam	AB-32386	1:100	Comet
CD146	Cell Signaling	81701	1:50, 1:100	Comet / IHC
F4/80	Cell Signaling	70076	1:100	Comet / IHC
β-catenin	Abcam	AB-224803	1:200	Comet
Vimentin	Abcam	AB-92547	1:1000	Comet
Glutamine synthetase	BD Biosciences	610518	1:2000, 1:1000	Comet / IHC
Anti-Rabbit AF555	ThermoFisher Scientific	A31572	1:100	Comet
Anti-Rabbit AF647	ThermoFisher Scientific	A21245	1:200	Comet
Anti-Mouse AF647	ThermoFisher Scientific	A21236	1:200	Comet
Anti-Rat AF647	ThermoFisher Scientific	A21247	1:200	Comet
Anti-Goat 647	ThermoFisher Scientific	A21446	1:200	Comet
KI67	ThermoFisher Scientific	MA5-14520	1:200	IHC
Cleaved caspase-3	Cell signaling	D175	1:600	IHC

Fig.1

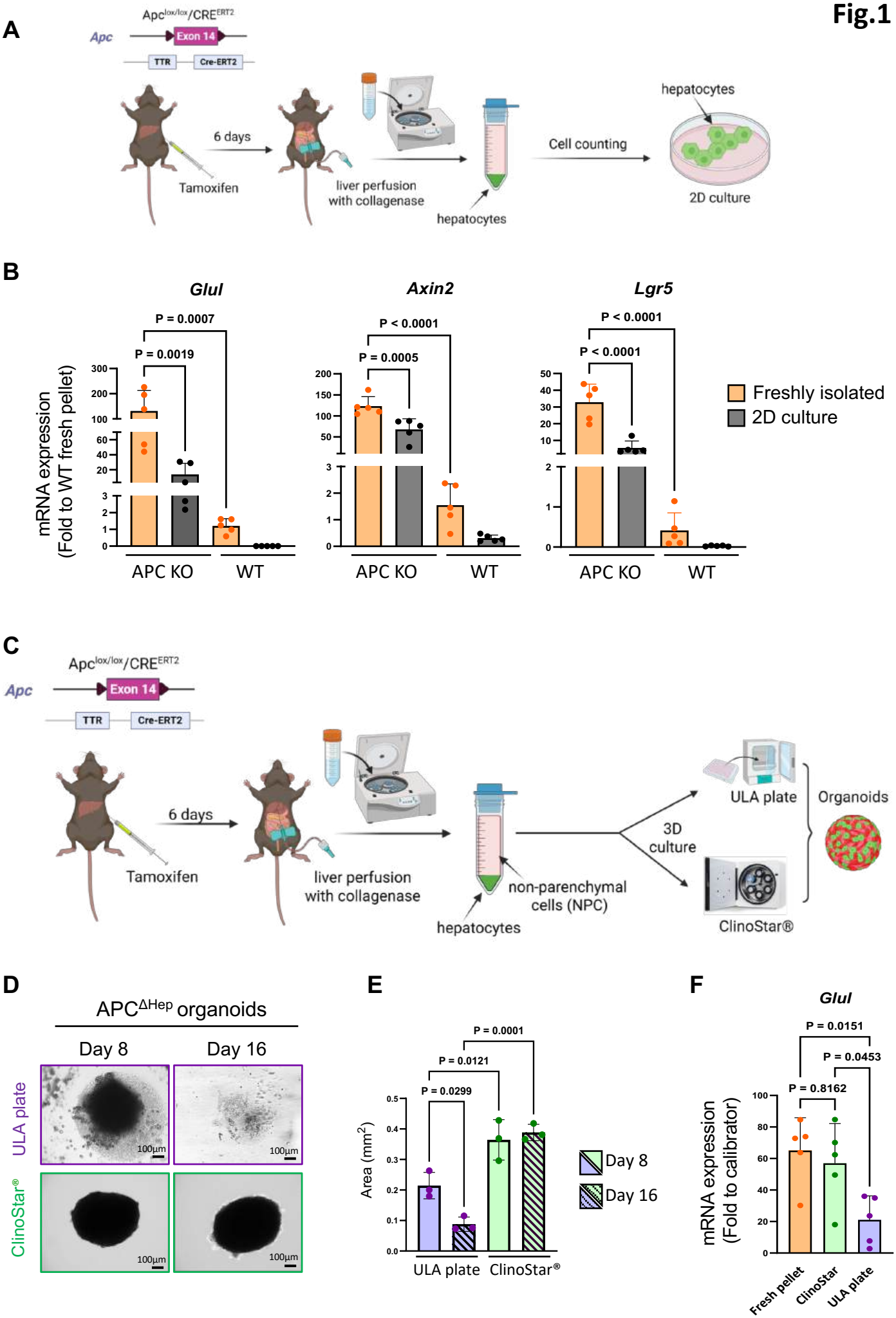
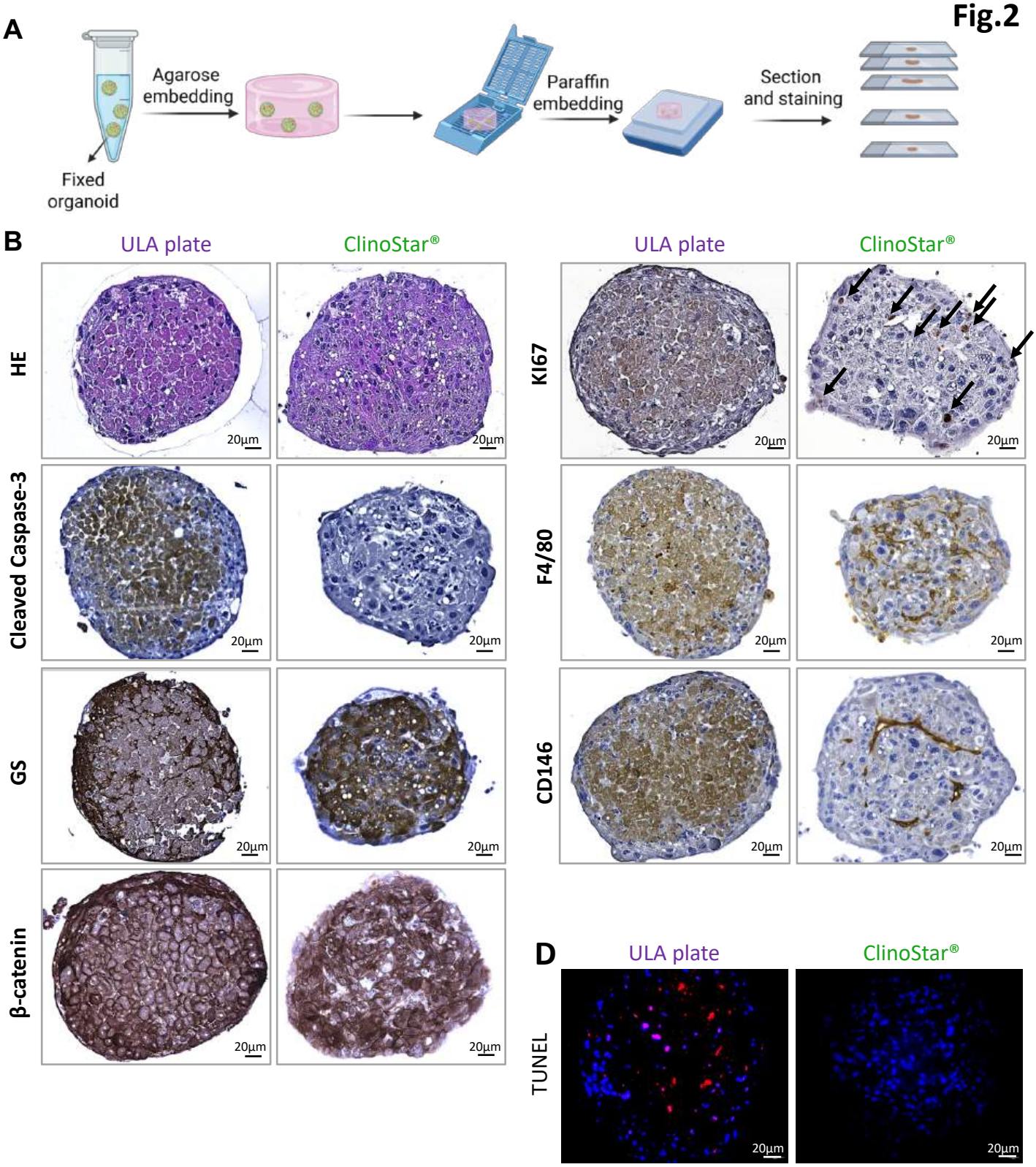
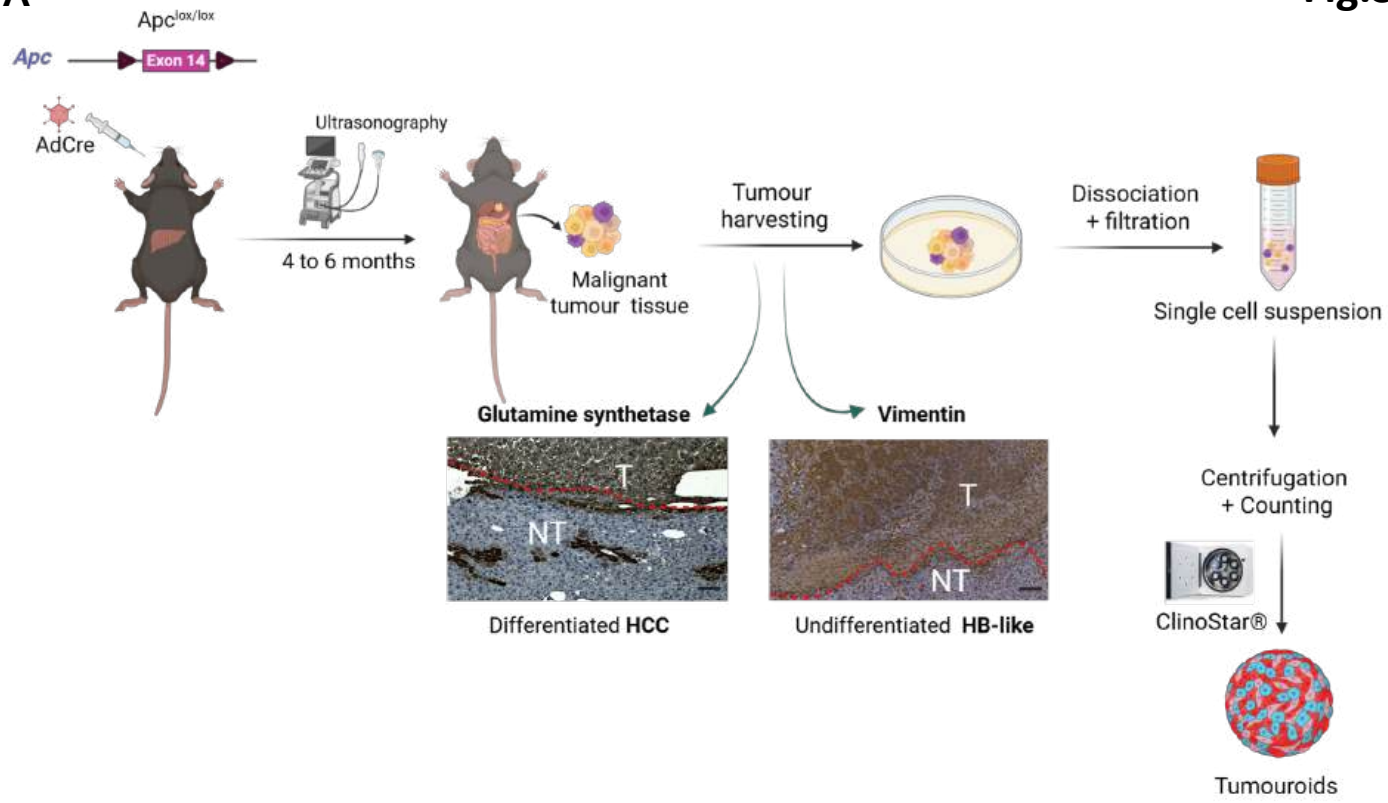

A
Apc lox/lox /CRE ERT2
Apc
Exon 14
TTR
Cre-ERT2
6 days
Tamoxifen
liver perfusion with collagenase
hepatocytes
Cell counting
hepatocytes
2D culture
B
Glul
Axin2
Lgr5
P = 0.0007
P = 0.0019
P < 0.0001
P = 0.0005
P < 0.0001
P < 0.0001
mRNA expression (Fold to WT fresh pellet)
Freshly isolated
2D culture
APC KO
WT
C
Apc lox/lox /CRE ERT2
Apc
Exon 14
TTR
Cre-ERT2
6 days
Tamoxifen
liver perfusion with collagenase
hepatocytes
non-parenchymal cells (NPC)
3D culture
ULA plate
ClinoStar®
Organoids
D
APC ΔHep organoids
Day 8
Day 16
ULA plate
ClinoStar®
100µm
E
P = 0.0001
P = 0.0121
P = 0.0299
Area (mm2)
Day 8
Day 16
ULA plate
ClinoStar®
F
Glul
P = 0.0151
P = 0.0453
P = 0.8162
mRNA expression (Fold to calibrator)
Fresh pellet
ClinoStar
ULA plate

Fig.2


A
Agarose embedding
Fixed organoid
Paraffin embedding
Section and staining
B
ULA plate
ClinoStar®
HE
Cleaved Caspase-3
GS
β-catenin
KI67
F4/80
CD146
20μm
D
TUNEL
C
KI67
Cleaved caspase-3
F4/80
CD146
P = 0.0312
P = 0.0022
P = 0.0043
P = 0.0312
KI67+/KI67- cells (%)
Cleaved Caspase-3+ cells/area (%)
F4/80+ cells/area (%)
CD146+ cells/area (%)
ULA plate
ClinoStar®

A


Apc lox/lox
Apc
Exon 14
AdCre
Ultrasonography
4 to 6 months
Malignant tumour tissue
Tumour harvesting
Dissociation + filtration
Single cell suspension
Centrifugation + Counting
ClinoStar®
Tumouroids
Glutamine synthetase
Vimentin
T
NT
Differentiated HCC
Undifferentiated HB-like

B

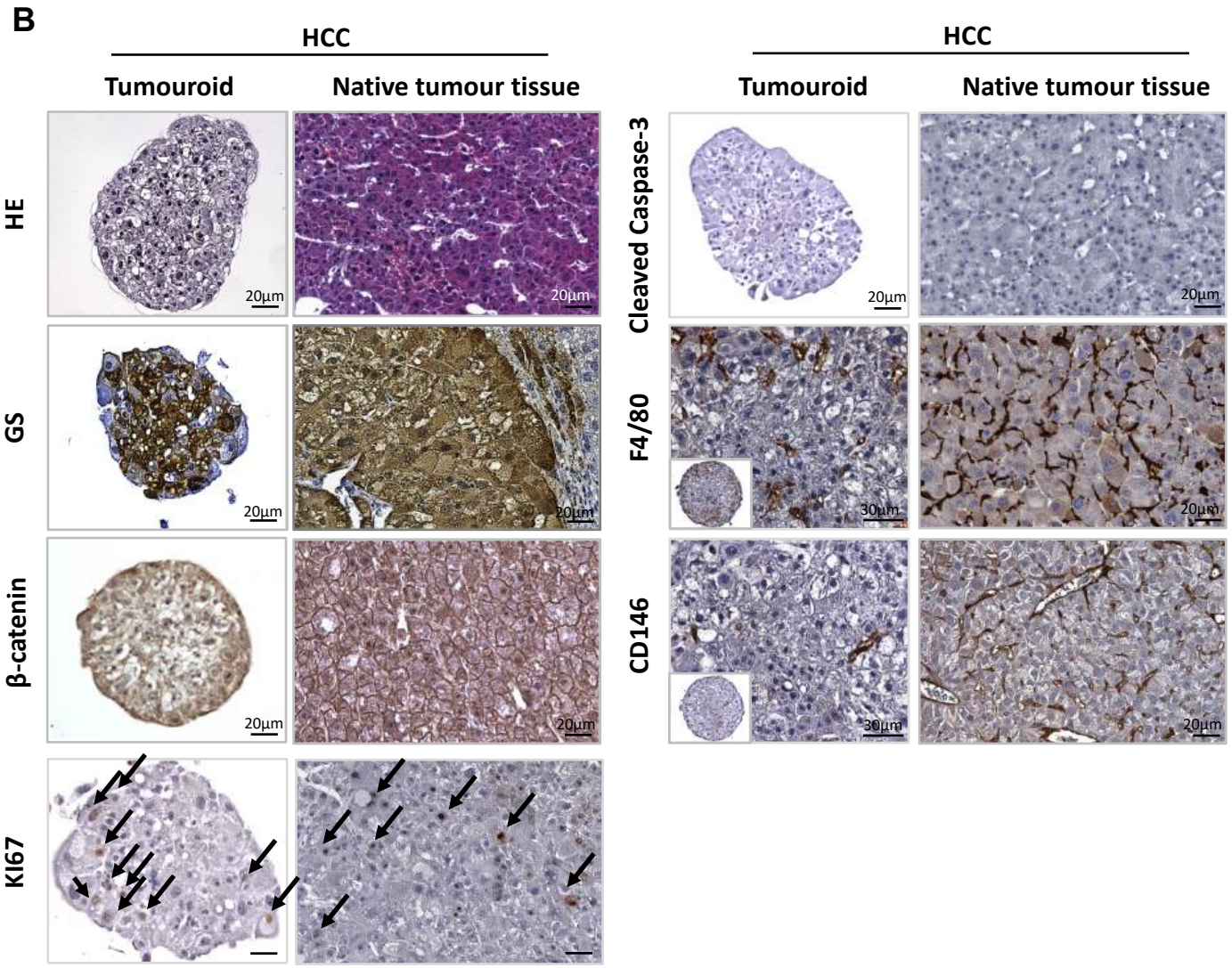
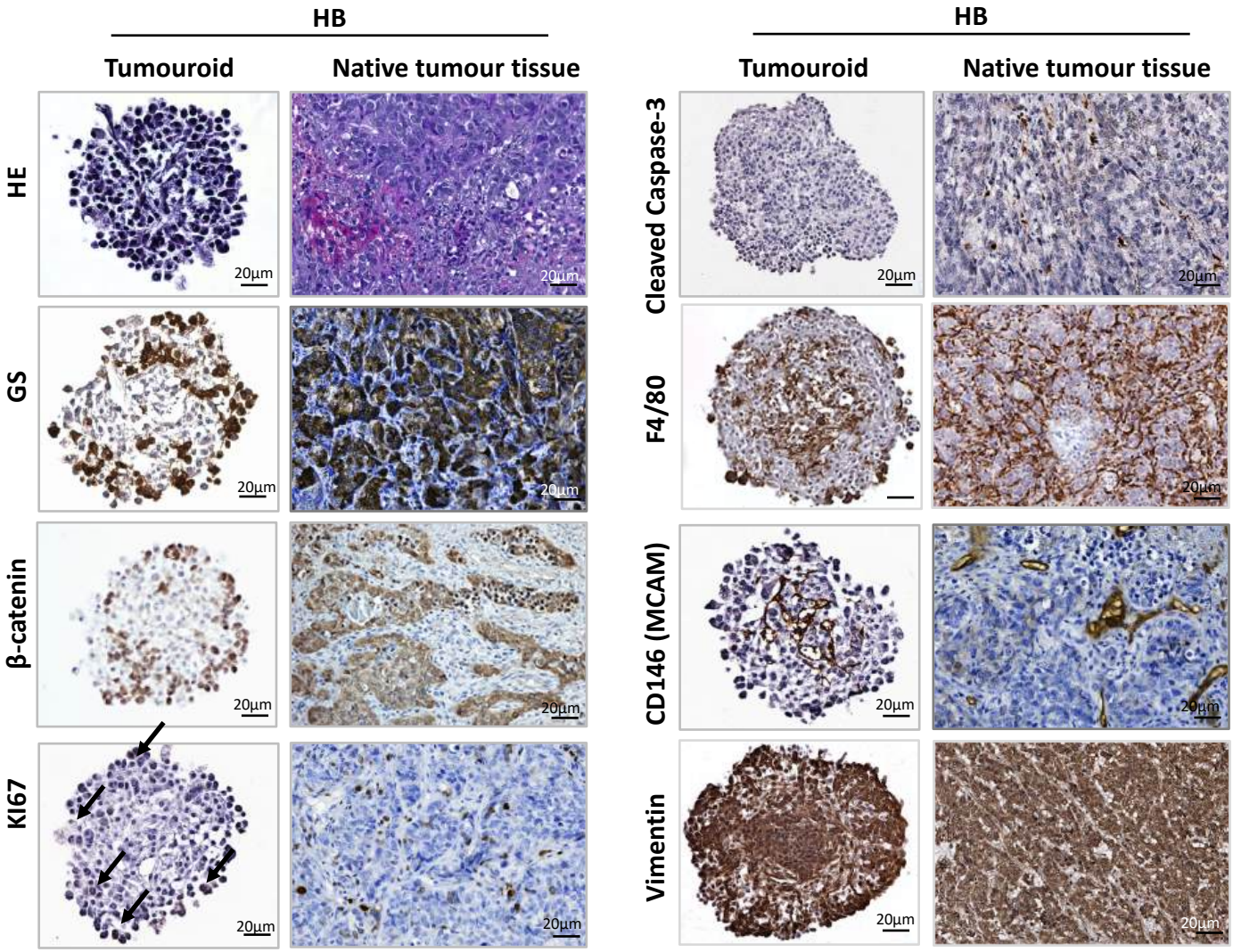

HCC
Tumouroid
Native tumour tissue
HE
GS
β-catenin
KI67
Cleaved Caspase-3
F4/80
CD146
20µm
30µm

Fig.4


HB
Tumouroid
Native tumour tissue
HE
GS
β-catenin
KI67
20μm
HB
Tumouroid
Native tumour tissue
Cleaved Caspase-3
F4/80
CD146 (MCAM)
Vimentin
20μm

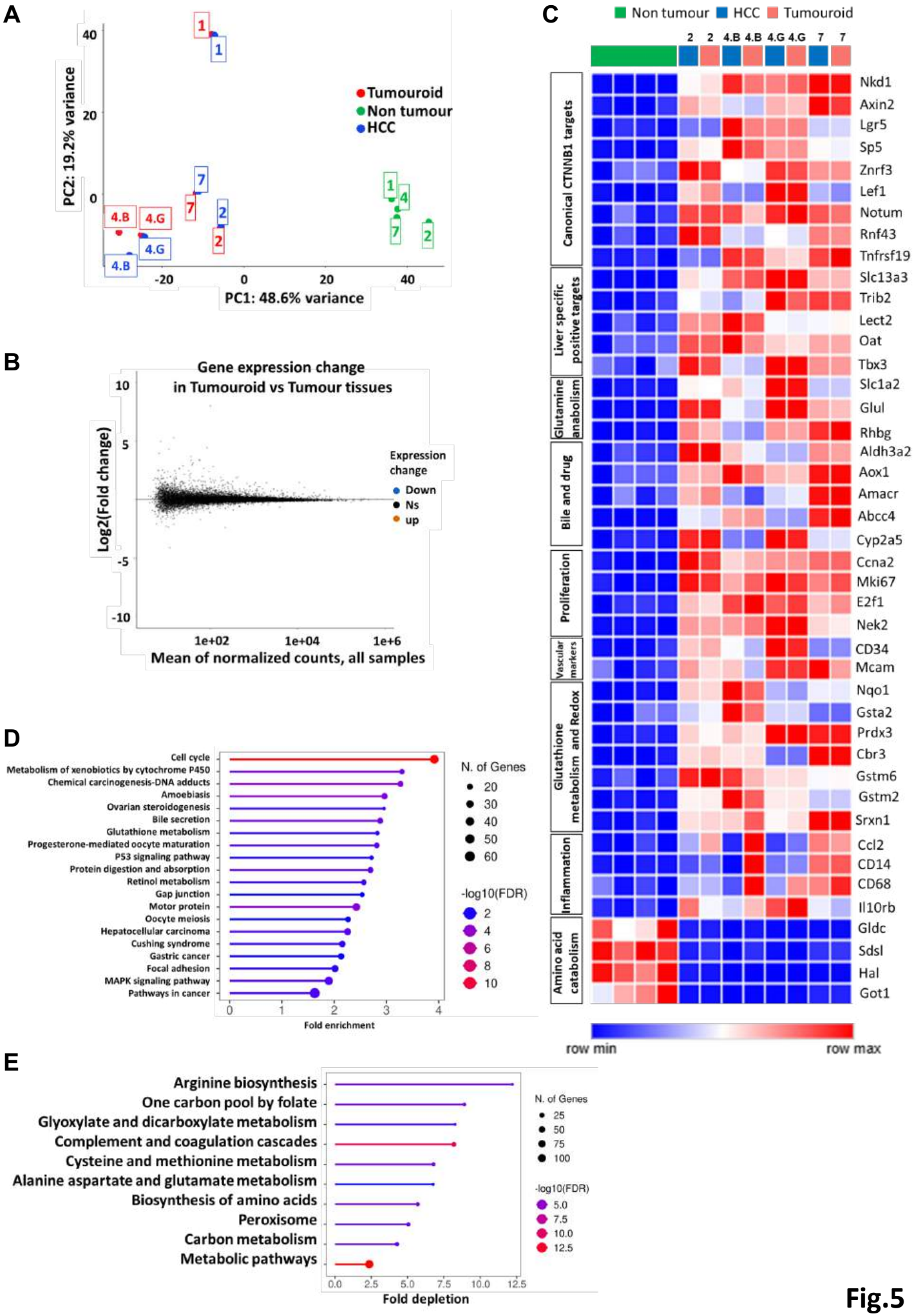

A
PC2: 19.2% variance
PC1: 48.6% variance
Tumouroid
Non tumour
HCC
B
Gene expression change
in Tumouroid vs Tumour tissues
Log2(Fold change)
Mean of normalized counts, all samples
Expression change
Down
Ns
up
C
Non tumour
HCC
Tumouroid
Canonical CTNNB1 targets
Liver specific positive targets
Glutamine anabolism
Bile and drug
Proliferation
Vascular markers
Glutathione metabolism and Redox
Inflammation
Amino acid catabolism
Nkd1
Axin2
Lgr5
Sp5
Znrf3
Lef1
Notum
Rnf43
Tnfrsf19
Slc13a3
Trib2
Lect2
Oat
Tbx3
Slc1a2
Glul
Rhbg
Aldh3a2
Aox1
Amacr
Abcc4
Cyp2a5
Ccna2
Mki67
E2f1
Nek2
CD34
Mcam
Nqo1
Gsta2
Prdx3
Cbr3
Gstm6
Gstm2
Srxn1
Ccl2
CD14
CD68
Il10rb
Gldc
Sdsl
Hal
Got1
row min
row max
D
Cell cycle
Metabolism of xenobiotics by cytochrome P450
Chemical carcinogenesis-DNA adducts
Amoebiasis
Ovarian steroidogenesis
Bile secretion
Glutathione metabolism
Progesterone-mediated oocyte maturation
P53 signaling pathway
Protein digestion and absorption
Retinol metabolism
Gap junction
Motor protein
Oocyte meiosis
Hepatocellular carcinoma
Cushing syndrome
Gastric cancer
Focal adhesion
MAPK signaling pathway
Pathways in cancer
Fold enrichment
N. of Genes
-log10(FDR)
E
Arginine biosynthesis
One carbon pool by folate
Glyoxylate and dicarboxylate metabolism
Complement and coagulation cascades
Cysteine and methionine metabolism
Alanine aspartate and glutamate metabolism
Biosynthesis of amino acids
Peroxisome
Carbon metabolism
Metabolic pathways
Fold depletion
N. of Genes
-log10(FDR)

Fig.5

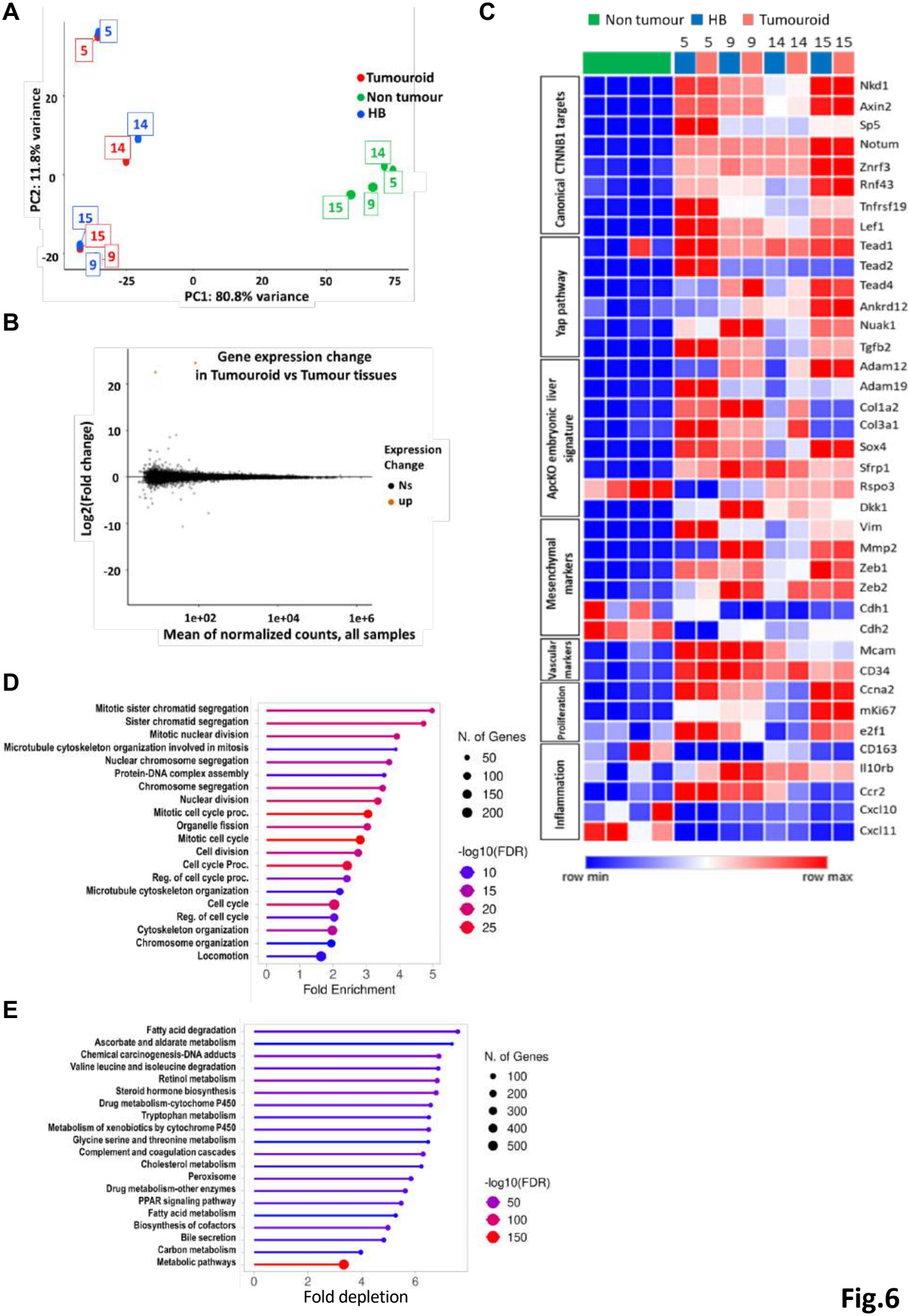

A
PC2: 11.8% variance
PC1: 80.8% variance
Tumouroid
Non tumour
HB
B
Gene expression change
in Tumouroid vs Tumour tissues
Log2(Fold change)
Mean of normalized counts, all samples
Expression Change
Ns
up
C
Non tumour
HB
Tumouroid
Canonical CTNNB1 targets
Yap pathway
ApcKO embryonic liver signature
Mesenchymal markers
Vascular markers
Proliferation
Inflammation
Nkd1
Axin2
Sp5
Notum
Znrf3
Rnf43
Tnfrsf19
Lef1
Tead1
Tead2
Tead4
Ankrd12
Nuak1
Tgfb2
Adam12
Adam19
Col1a2
Col3a1
Sox4
Sfrp1
Rspo3
Dkk1
Vim
Mmp2
Zeb1
Zeb2
Cdh1
Cdh2
Mcam
CD34
Ccna2
mKi67
e2f1
CD163
Il10rb
Ccr2
Cxcl10
Cxcl11
row min
row max
D
Mitotic sister chromatid segregation
Sister chromatid segregation
Mitotic nuclear division
Microtubule cytoskeleton organization involved in mitosis
Nuclear chromosome segregation
Protein-DNA complex assembly
Chromosome segregation
Nuclear division
Mitotic cell cycle proc.
Organelle fission
Mitotic cell cycle
Cell division
Cell cycle Proc.
Reg. of cell cycle proc.
Microtubule cytoskeleton organization
Cell cycle
Reg. of cell cycle
Cytoskeleton organization
Chromosome organization
Locomotion
Fold Enrichment
N. of Genes
-log10(FDR)
E
Fatty acid degradation
Ascorbate and aldarate metabolism
Chemical carcinogenesis-DNA adducts
Valine leucine and isoleucine degradation
Retinol metabolism
Steroid hormone biosynthesis
Drug metabolism-cytochome P450
Tryptophan metabolism
Metabolism of xenobiotics by cytochrome P450
Glycine serine and threonine metabolism
Complement and coagulation cascades
Cholesterol metabolism
Peroxisome
Drug metabolism-other enzymes
PPAR signaling pathway
Fatty acid metabolism
Biosynthesis of cofactors
Bile secretion
Carbon metabolism
Metabolic pathways
Fold depletion
N. of Genes
-log10(FDR)

Fig.6

Fig.7

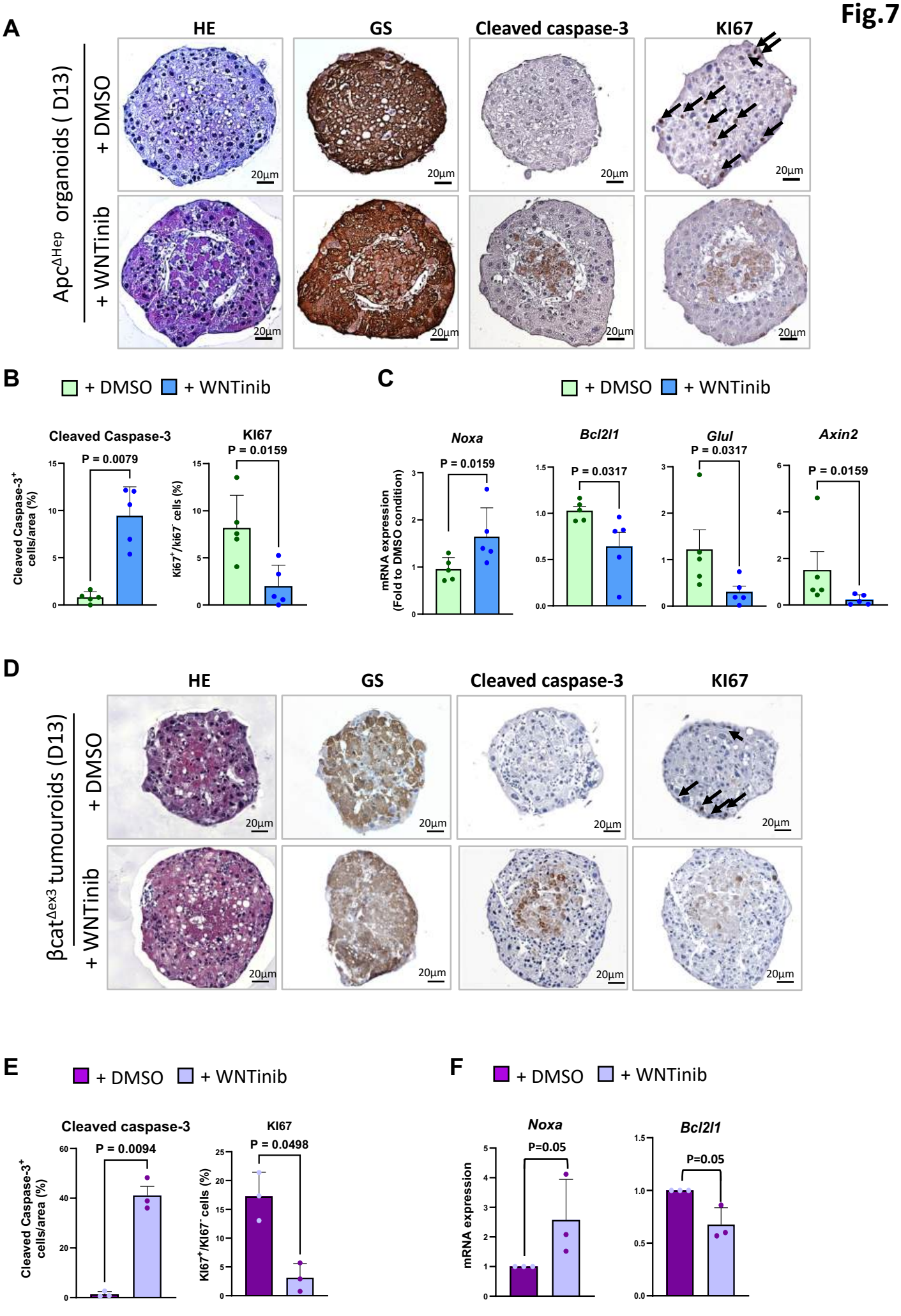

A
HE
GS
Cleaved caspase-3
KI67
Apc^ΔHep organoids (D13)
+ DMSO
+ WNTinib
20µm
B
+ DMSO
+ WNTinib
Cleaved Caspase-3
P = 0.0079
Cleaved Caspase-3+ cells/area (%)
KI67
P = 0.0159
Ki67+/ki67- cells (%)
C
+ DMSO
+ WNTinib
Noxa
P = 0.0159
Bcl2l1
P = 0.0317
Glul
P = 0.0317
Axin2
P = 0.0159
mRNA expression (Fold to DMSO condition)
D
HE
GS
Cleaved caspase-3
KI67
βcat^Δex3 tumouroids (D13)
+ DMSO
+ WNTinib
20µm
E
+ DMSO
+ WNTinib
Cleaved caspase-3
P = 0.0094
Cleaved Caspase-3+ cells/area (%)
KI67
P = 0.0498
KI67+/KI67- cells (%)
F
+ DMSO
+ WNTinib
Noxa
P=0.05
Bcl2l1
P=0.05
mRNA expression

Fig.S1

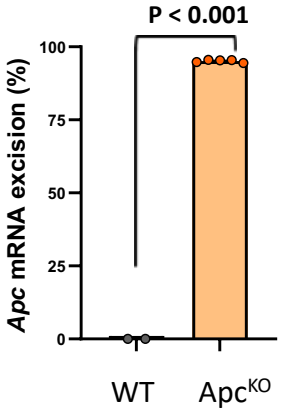


Fig.S2

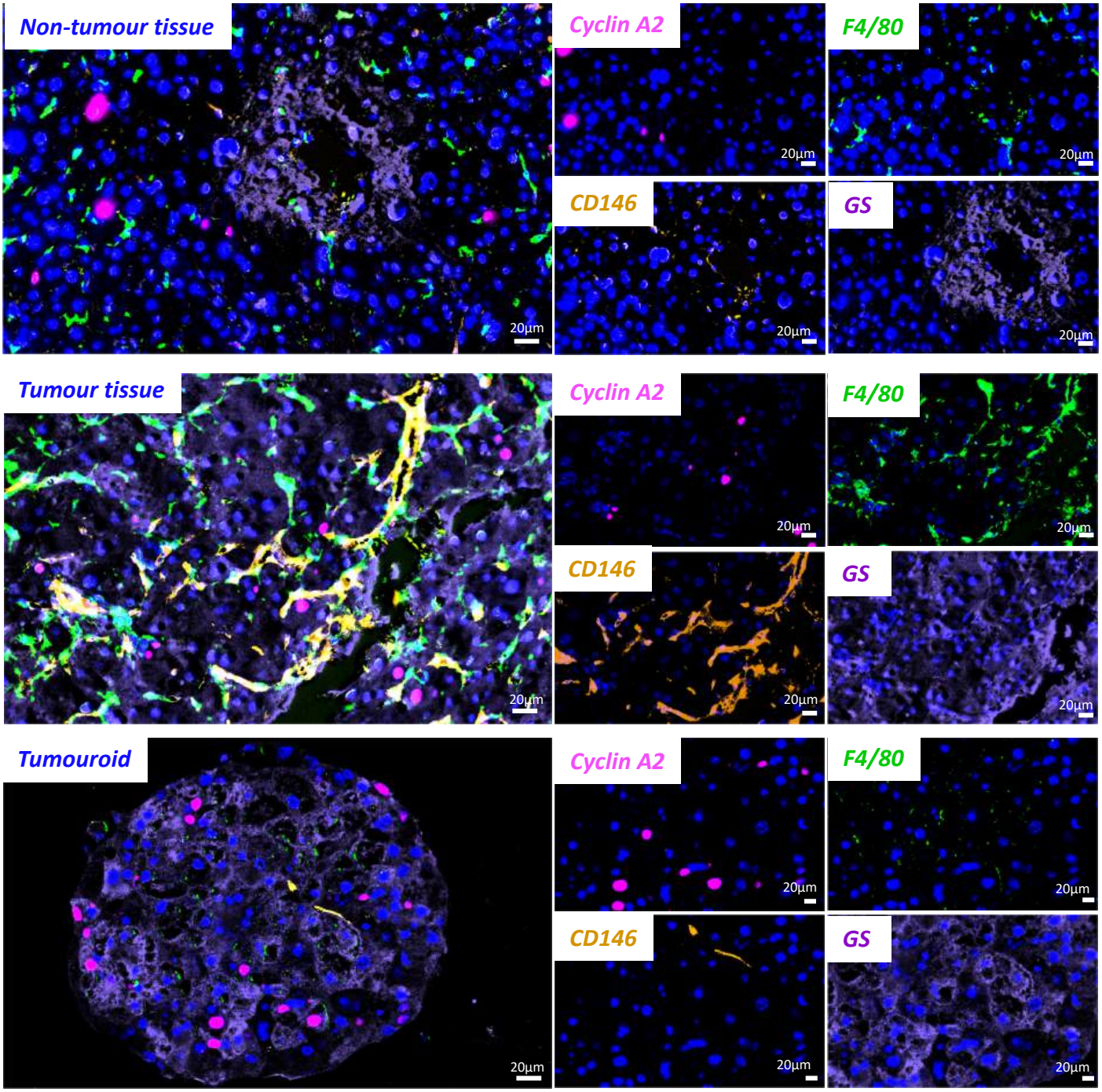

Non-tumour tissue
Cyclin A2
F4/80
CD146
GS
Tumour tissue
Cyclin A2
F4/80
CD146
GS
Tumouroid
Cyclin A2
F4/80
CD146
GS
20μm

Fig.S3

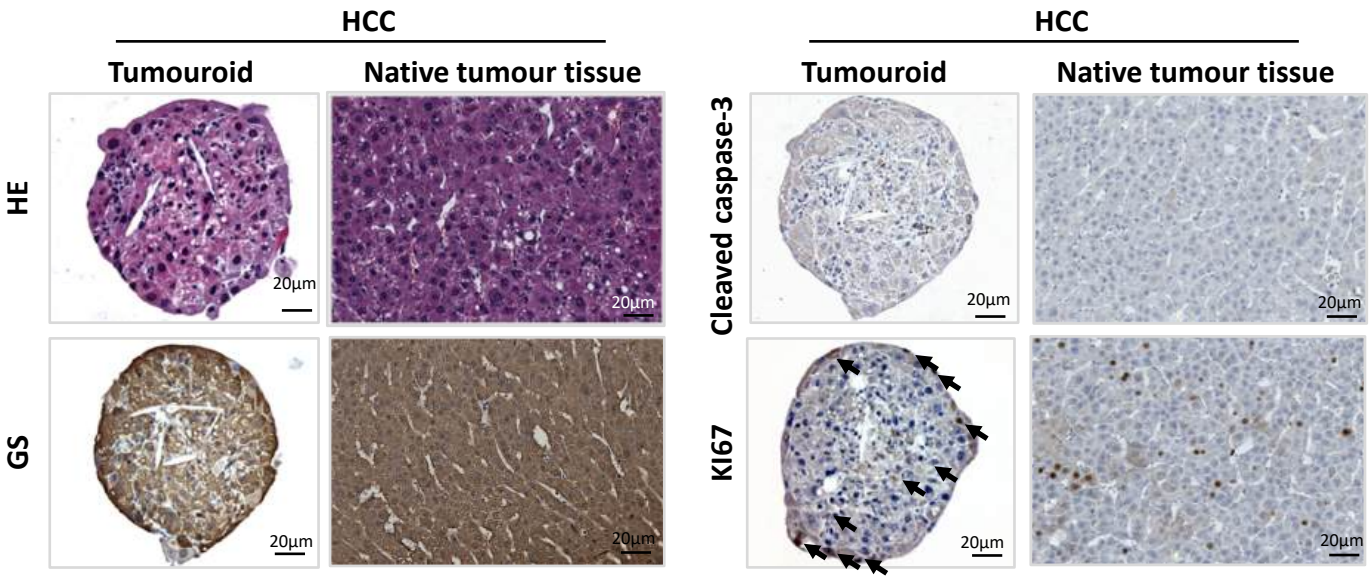
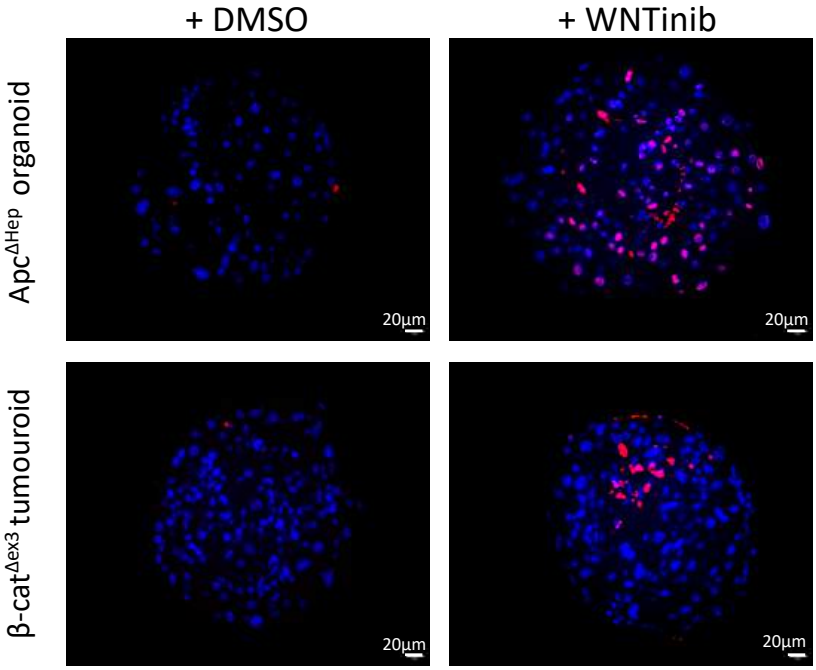

HCC
Tumouroid
Native tumour tissue
HE
GS
20μm
HCC
Tumouroid
Native tumour tissue
Cleaved caspase-3
KI67
20μm

Fig.S4


+ DMSO
+ WNTinib
Apc^ΔHep organoid
β-cat^Δex3 tumouroid
20µm
20µm
20µm
20µm